Effects of Temperature on the Proliferation of Human and Fish Lens Epithelial Cells

by

Ziqing Li

A thesis
presented to the University of Waterloo
in fulfillment of the
thesis requirement for the degree of
Master's of Science
in
Vision Science

Waterloo, Ontario, Canada, 2019

Author's Declaration

I hereby declare that I am the sole author of this thesis. This is a true copy of the thesis, including any required final revisions, as accepted by my examiners.

I understand that my thesis may be made electronically available to the public.

Abstract

Crystallins are proteins that confer refractive properties to the crystalline lens. All vertebrate lenses contain α- and β-crystallins, and often a third major crystallin. Crystallins can have additional non-refractive functions; α-crystallins act as heat shock proteins, protecting lenses from heat-induced denaturation, and γ-crystallins are thought to be cryoproteins, protecting lenses from extreme cold. The concentration of α-crystallins is higher in mammalian lenses than in teleost lenses, while the opposite is true for γ-crystallins, suggesting that mammalian lenses would be better protected in warmer conditions and teleost lenses better protected in colder temperatures. This study determined whether temperature affects the growth of lens epithelial cells (LECs) derived from human and fish lenses. Both human and rainbow trout fish LECs were cultured (n = 4 each) and grown for 1, 2, 4, 6, 8 and 12 days at the optimal (37°C and 18°C, respectively), higher than optimal (42°C and 25°C, respectively) and lower than optimal temperatures (32°C and 10°C, respectively). At optimal temperatures, both fish and human LECs grew optimally. Higher temperatures were more deleterious to the proliferation index than lower temperatures for both human and fish LECs. Mitotic cells were non-existent in fish LECs grown at high temperatures. The sizes of the cells did not greatly change with temperature with either species, but human cells at non-optimal temperature tended to clump over time. Human LECs at the optimal temperature maintained their random distribution. Fish LECs at optimal temperatures moved from a random distribution to a clumped distribution, but lower temperatures had the opposite effect; LECs moved from a clumped to a random distribution. Only the high temperature group of fish LECs maintain their random organisation.

Acknowledgements

I could write another thesis about the people I would like to thank. But I love the environment, so I must save paper.

I would like to express my sincere gratitude to Dr. Vivian Choh and Dr. Jacob Sivak for their unlimited support and guidance throughout this research. Their motivation, enthusiasm and immense knowledge towards Vision Science has inspired me deeply. It was a great privilege and honour to study under their guidance. I could not have imagined the greatest of mentors for my M.Sc. study.

My sincere thankfulness goes to my committee for their continued support and encouragement: Dr. David McCanna and Dr. Denise Hileeto. Also, I would like to give special thanks to Miriam Heyen, Daryl Enstone and Stephanie and Holly Forsyth for their unconditional help during the whole of my master's degree.

The completion of this study could not have been accomplished without the fantastic support of family, peers, faculty members, and current Optometry undergrads. And to all my friends, without you, I would have graduated earlier.

Mucho Amor.

Dedication

To my father: for his patience, advice, guidance, and understanding.

To be honest, I don't think dad will ever read this. Which is good, because then mum will be jealous, and she'll want me to do a Ph.D.

Table of Contents

List of Figures

List of Tables

List of Abbreviations

α ..... alpha

β ..... beta

δ ..... delta

γ ..... gamma

ANOVA ..... analysis of variance

ATCC ..... American Type Culture Collection

ATPase ..... sodium-potassium adenosine triphosphatase

BSA ..... bovine serum albumin

CDK ..... cyclin-dependent kinases

CN III ..... oculomotor nerve

CO_2 ..... carbon dioxide

COI ..... cell of interest

Cps ..... count per second

$CuSO_4$ ..... cupric sulfate pentahydrate

DAPI ..... 4′,6-diamidino-2-phenylindole

DIOC(6) ..... 3,3′-dihexyloxacarbocyanine iodide

DMEM/F12 ..... Dulbecco's modified eagle medium F-12

DMSO ..... dimethyl sulfoxide

DNA ..... deoxyribonucleic acid

EMT ..... epithelial to mesenchymal transition

dps ..... days post seeding

EdU ..... 5-ethynyl-2'-deoxyuridine

F(ab) ..... antigen-binding fragment

FBS ..... fetal bovine serum

G_0 ..... resting phase

G_1 ..... gap 1 phase

G_2 ..... gap 2 phase

hγS ..... human γs-crystallin

IgG ..... immunoglobulin g

JAM ..... junction adhesion molecules

kDa ..... kilodalton

L-15 ..... Leibovitz L-15

LECs ..... lens epithelial cells

LGN ..... lateral geniculate nucleus

M ..... mitosis phase

Macro ..... macroinstruction

MET ..... mesenchymal to epithelial transition

nm ..... nanometer

ºC ..... degrees Celsius

PCO ..... posterior capsular opacification

pen-strep ..... penicillin-streptomycin

PFA ..... paraformaldehyde

rcf ..... relative centrifugal force

ROI ..... region of interest

ROS ..... reactive oxygen species

rpm ..... rotation per minute

RT ..... room temperature

S ..... synthesis

SCN ..... suprachiasmatic nucleus

SEM ..... standard error of the mean

TBS ..... Tris buffered saline

TJ ..... tight junction

TRITC ..... tetramethylrhodamine isothiocyanate

TRP ..... tryptophan

TγS1 ..... *D. mawsoni* γs1-crystallin

TγS2 ..... *D. mawsoni* γs2-crystallinA

UV ..... ultraviolet

WIS ..... water-insoluble

WS ..... water soluble

ZO ..... zonula occludin

ZO-1 ..... zonula occludin 1

I. LITERATURE REVIEW

1.1 THE EYE

The human body consists of many organ systems that work together and depend directly or indirectly on one another to build a functional organism. One of the most complex sensory organs among all animals is the eye; it can turn sensory information (i.e., light rays from the surrounding environment) into electrical and chemical signals that are relayed to the brain.

Numerous types of eyes exist in nature, and they can be categorized into simple and compound; the simplest invertebrate eyes have one photoreceptive surface. Simple eyes include pit eyes, pinholes, and eyes with spherical lenses among others. Compound eyes in invertebrates are only present in arthropods and are categorized into apposition and superposition compound eyes (Land & Fernald, 1992). Compound eyes contain more than one ommatidium, which are isolated units containing a one or two refractive elements that focus light onto light-absorbing pigment. In an apposition compound eye, each light receptor cell receives an image from one ommatidium; given that the number of ommatidia can be as many as 2000, images from these eyes are usually sharper. In superposition compound eyes, each receptor cell receives images from more than one neighbouring ommatidia. Superposition eyes are usually found in nocturnal animals because the light absorbed by each receptor cells can be obtained by multiple (neighbouring) ommatidia but at the cost of some resolution (Warrant, 2017).

The vertebrate eye is composed of three layers, namely outer, middle, and inner. The outer fibrous layer forms the sclera and cornea. The sclera is a sturdy white opaque

tissue that encircles and protects the eye from damage, and furthermore, it is an attachment point for extraocular muscles that are responsible for moving the eyeball. The cornea is continuous with the sclera and is transparent and avascular, which allows light rays to enter easily (Purves *et al.*, 2001).

The cornea is composed of the following five layers: the epithelium, Bowman's layer, stroma, Descemet's membrane, and the endothelium (from anterior to posterior, respectively). The outermost epithelium is approximately five to seven cells thick comprising a stratified corneal epithelium, wing cells, and a basal cell layer. Bowman's layer, beneath the epithelial cells, is an acellular, nonregenerative layer made up of collagen fibrils (Remington & Remington, 2012); its primary function has yet to be discovered (Wilson & Hong, 2000). The stroma is the thickest layer and is located in the center of the cornea. It is composed of collagen fibrils, keratocytes, and extracellular ground substance; these contribute to most of the cornea's thickness as well as its transparency (Maurice, 1957). Descemet's membrane consists of anterior and posterior lamellae, which can regenerate, thereby maintaining the function and equilibrium of the corneal endothelial cells (J. Chen *et al.*, 2017). Another function of Descemet's membrane is to resist trauma and substances from the external environment that may be pathological to the ocular body (Remington & Remington, 2012). The endothelium is the innermost layer of the cornea and is composed of a single layer of polyhedral and hexagonal cells that form a honeycomb-like structure. Several junctions exist between these cells; however, the endothelium is relatively permeable because the cell walls have Na^+-K^+-ATPase pumps that can regulate the water content of all layers of the cornea, the basal layer of the endothelium has numerous hemidesmosomes (DelMonte & Kim, 2011).

The limbus is the border between the cornea and sclera; it contains the canal of Schlemm, which is a major drain for the aqueous humour (Van Buskirk, 1989).

The uvea, the pigmented three-layered middle vascular layer of the eye, is made up of the iris, ciliary body, and choroid. The iris is the coloured portion of the eye and defines the diameter of the pupil. The size of the pupil is regulated by the dilator and sphincter muscles of the iris, which respectively enlarge and constrict the diameter of the pupil via the autonomic nervous system. The ciliary body is an extension of the iris and has a ring of muscles that can indirectly adjust the shape of the lens for accommodation; it is also responsible for producing aqueous humour. The choroid is a vascular structure capable of providing blood and nutrients to the outer retina (Nickla & Wallman, 2010; Purves, D *et al.*, 2001; Remington & Remington, 2012).

The retina develops from the neural ectoderm. It is composed of two layers: an outer pigmented layer (tightly attached to the choroid) and a neural retina (attached to the pigmented epithelium) (Purves *et al.*, 2001). Five types of neurons are present in the retina: photoreceptors, bipolar cells, ganglion cells, horizontal cells, and amacrine cells (Purves *et al.*, 2001). The Müller cells are another cell type that is considered a support cell for the retina. The various cells ultimately transduce light into electrical signals that are then sent to the central nervous system via the axons that comprise the optic nerve fibres.

The eye has three structural chambers, namely the anterior, posterior, and vitreous chambers. The anterior chamber is bound by the cornea, iris, and lens, whereas the posterior chamber encircles the lens, behind the iris. The aqueous humour circulates between these two chambers, supplying nutrients to avascular tissues such as the

posterior cornea and lens (McCaa, 1982). The vitreous chamber is defined by the space between the back of the lens and the retina, and contains the vitreous humour, which constitutes 80% of the eye's volume and has multiple functions, such as maintaining the eye structure, removing debris, and providing nutrients (Purves *et al.*, 2001).

Light enters through the cornea and passes through the anterior chamber. The iris sphincter and dilator muscles alter the pupil's size, which allows the optimal amount of light to enter and thus avoids damaging the retina (Remington, 2005), when the light entering the eye is too bright, the sphincter muscles contract via the oculomotor nerve (CN III), which in turn constricts the pupil (Joyce & Peterson, 2019). In contrast, when the light is too dim, the iris dilator muscle contracts to allow more light to reach the retina; the dilator muscle is controlled by the sympathetic system (Pilar *et al.*, 1987). The lens refracts a precise amount of light and focusses light on the retina. Photoreceptors in the retina transduce the light into electrical signals, and the signals are and relayed through bipolar and ganglion cells to the ganglion cells (Joukal, 2017). Axons from the retinal ganglion cells run together to form the optic nerve. Visual information leaves the eyes through the optic nerve, before being transported to the lateral geniculate nucleus, a significant relay center in the brain. Fibres from the LGN form optic radiation that head towards the visual cortex for processing (Joukal, 2017). The visual cortex contains the Brodmann areas 17 (striate area), 18 (parastriate area), and 19 (peristriate area), which are responsible for visual processing in the occipital lobe (Remington, 2005). The posterior left and right hemispheres of the brain are each responsible for only the contralateral visual field; that is, the right hemisphere receives information from the left visual field and vice versa (Figure 1).

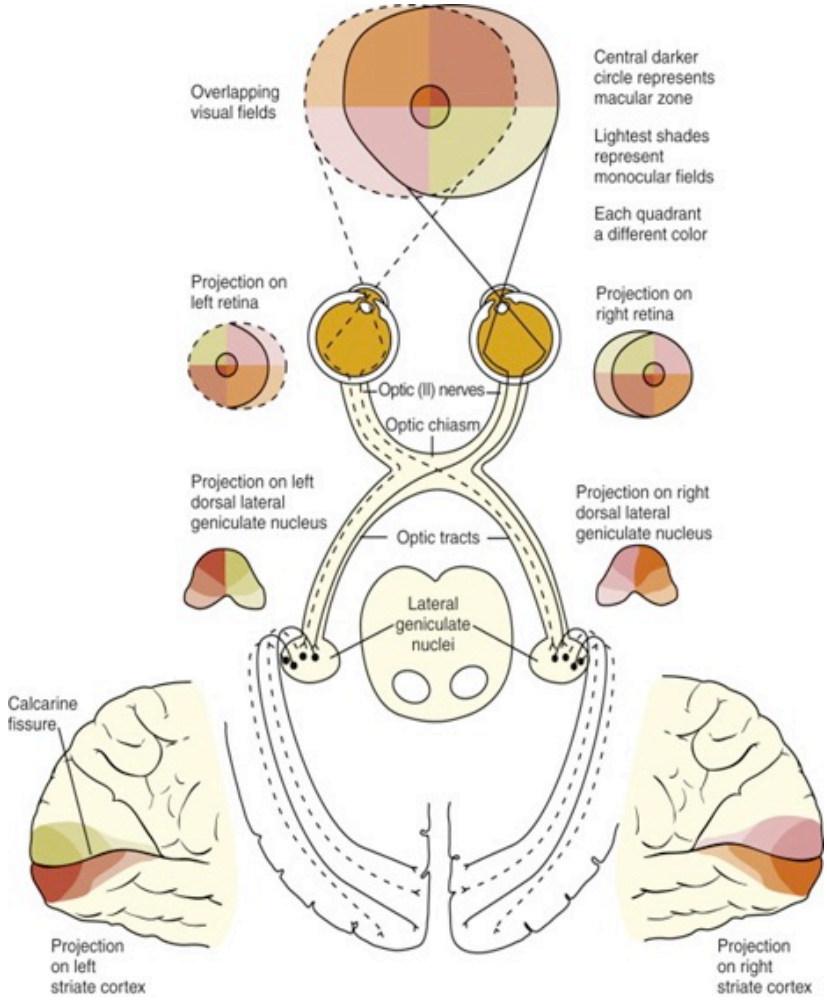

Figure 1: The visual pathway. Reprinted from Clinical Anatomy and Physiology of the Visual system, 3rd edition, Remington L.A., Chapter 13–Visual Pathway, pages 233–252, Copyright (2012), with permission from Elsevier.

1.2 EMBRYOLOGY OF THE HUMAN EYE

The development of the eye begins by the third week of pregnancy as part of the neurulation process in the rest of the body. The ectoderm thickens to create a neural plate, which then invaginates, forming neural folds. Optic pits, evaginations within the neural folds also form and eventually the neural folds fuse, forming the neural tube. Neural crest cells also form during this time; these cells eventually develop into mesenchymal cells. Although the neural tube originates from the ectoderm, it is referred

to as the neural tube of the neural ectoderm, making it easier to distinguish it from the surface ectoderm (Oyster, 1999).

The optic pits expand and then invaginate, forming the optic vesicles by the fourth week of pregnancy; the surface ectoderm next to the optic vesicle elongates and creates a lens placode (Adler & Canto-Soler, 2007). Both the optic vesicle and lens placode eventually the optic cup and lens vesicle, respectively (Oyster, 1999). The optic cup consists of an anterior and posterior sections. The anterior rim covers one-fifth of the cup, and the posterior makes up the remainder of the cup (Figure 2).

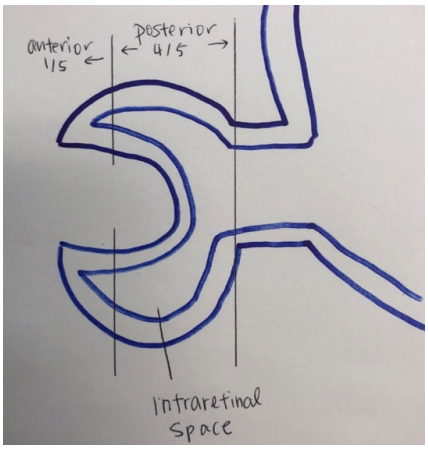

Figure 2: Division of the optic cup. Hand drawn, not to scale.

The anterior rim develops into the iris, and folds form along the rim into the *pars ciliaris retinae*, which eventually produces the ciliary body. The *pars ciliaris retinae* folds, resulting in the creation of the ciliary muscle from the mesenchymal cells that surround the anterior rim of the optic cup (Barrio-Asensio *et al.*, 2002; Davis-Silberman & Ashery-Padan, 2008).

The posterior part of the cup, which forms into the retina, also has an inner and outer layer. These layers differentiate into the neural retina and retinal pigmented epithelium, respectively (Cvekl & Tamm, 2004). From the sixth week of pregnancy, the retina begins to differentiate outward from the center towards the peripheral. Following detachment and differentiation of the lens vesicle from the surface ectoderm,

mesenchymal cells migrate between the anterior epithelium of the lens vesicle and the surface ectoderm. Ultimately, junctional complexes join posterior mesenchymal cells to form an endothelial monolayer.

The surface ectoderm becomes the corneal epithelium, the endothelial monolayer becomes the corneal endothelium, and the mesenchymal cells differentiate into corneal stroma fibroblasts, which comprise the cornea's specialized extracellular matrix. As the pattern develops in the corneal stroma, the cornea becomes transparent (Cvekl & Tamm, 2004).

The crystalline lens begins to develop during embryogenesis, and is a transparent, elliptical, and avascular tissue. It is one of two refractive elements of the eye and has a dioptric power of 60D in the human eye (Oyster, 1999). The elongated cells are called primary lens fibres, fill the posterior wall of the ectoderm, and elongate towards the lens vesicle. The anterior vesicle wall develops into the anterior subcapsular epithelial layer, which remains a stable monolayer throughout life (Mann, 1928; McAvoy *et al.*, 1999). Primary lens fibres remain at the center of the lens. Initially, proliferation of secondary lens fibre cells is very quick and growth and differentiation occurs at the germinative and transitional zone, respectively; however, as an individual age, proliferation slows down. Cells migrate to the transitional zone where they withdraw from the cell cycle, lose their organelles, and accumulate crystallins. These lens fibres are referred to as secondary lens fibres, and they differentiate throughout life, encircling the older fibres (Andley, 2008; Mann, 1928). As the secondary lens fibres grow, the end of one fibre meets with the beginning of another near the anterior and posterior poles. The regions where they meet are called sutures. Sutures vary in shape and size depending on the species; for example,

frogs and rabbits have line sutures, whereas humans have Y-shaped sutures (Brown *et al.*, 1989; Kuszak *et al.*, 2004; Willekens & Vrensen, 1982). Eight weeks into gestation, sutures become noticeable on both the anterior and posterior sides of primate lenses (Kuszak *et al.*, 1984). As time progresses, these sutures become more complex with more branches, and may even develop into star sutures.

Lastly, the adult lens nucleus contains the embryonic and fetal nuclei as well as more secondary lens fibres, which are created from the postnatal period to adolescence (Remington, 2005; Taylor *et al.*, 1996).After sexual maturity in most vertebrates, the lens cortex continues to expand and can be generally divided into three zones: superficial, internal, and deep (Augusteyn, 2010)

The rapid growth of the lens occurs from birth until the first year, and then the growth rate slows. By the time a child is 10 years old, the development of the lens slows significantly (Li & Ding, 2017). The human lens weighs approximately 90 mg at birth and increases by 1.38 mg every year because of the increase in secondary lens fibres (Augusteyn, 2004).

Any abnormalities during the embryonic development of the lens may lead to failure or abnormal growth, such as congenital cataracts, which result in the loss of transparency in the lens at birth and opacity of the lens caused by microarchitectural damage. Cataracts are the leading cause of blindness worldwide (Lepcha *et al.*, 2019). Multiple reasons for cataracts exist, based on the location or circumstances that caused opacification (Andley, 2008). In current times, surgery can be performed to remove the old lens and replace it with an artificial lens called an intraocular lens. However, recurring cataracts are observed in 50% of surgeries (Andley, 2008). Most of these

secondary cataracts are posterior capsular opacifications, which occur lens cells left behind from the original lens clump and obstruct vision (Liu *et al.*, 2012).

1.3 Comparison Between Human and Fish Lenses

Variations in vertebrate eyes depend on many factors, such as whether the species is diurnal, nocturnal, predatory, prey, terrestrial, or marine. The ocular lens can differ in shape, elasticity, and size; however, all healthy lenses are transparent with curved surfaces that refract light. A gradient of refractive index is also present in vertebrate lenses; refractive powers are higher in the center and lower in the periphery, the latter closely matching the refractive index of water (Jagger, 1992; Land, 2005).

Furthermore, the shape of the lens differs, depending on the environment that the species inhabits. Two main lens shapes exist, namely spherical and ovoid. Spherical lenses are generally seen in either aquatic or nocturnal animals. Most fish have spherical lenses that are solid and non-malleable (Prince, 1956). The lenses of rainbow trout tend to have a low radius of curvature, meaning a more spherical lens and a shorter focal length for the aquatic environment. They have a higher lens power and a higher gradient of refractive index. The corneal refractive power in aquatic animals is neutralized in water, and thus the lens is the only refractive element; this is in contrast to humans in which both the lens and cornea refract light (Sivak, 1990).

Ovoid lenses are seen mostly in terrestrial animals, such as monkeys. The power of the lens tends to be lower in mammals and birds. The lens of an amphibian changes shape as the tadpole metamorphoses into an adult. Tadpoles, with spherical lenses, spend most of their time in an aquatic environment, whereas adults, with ovoid lenses, live on

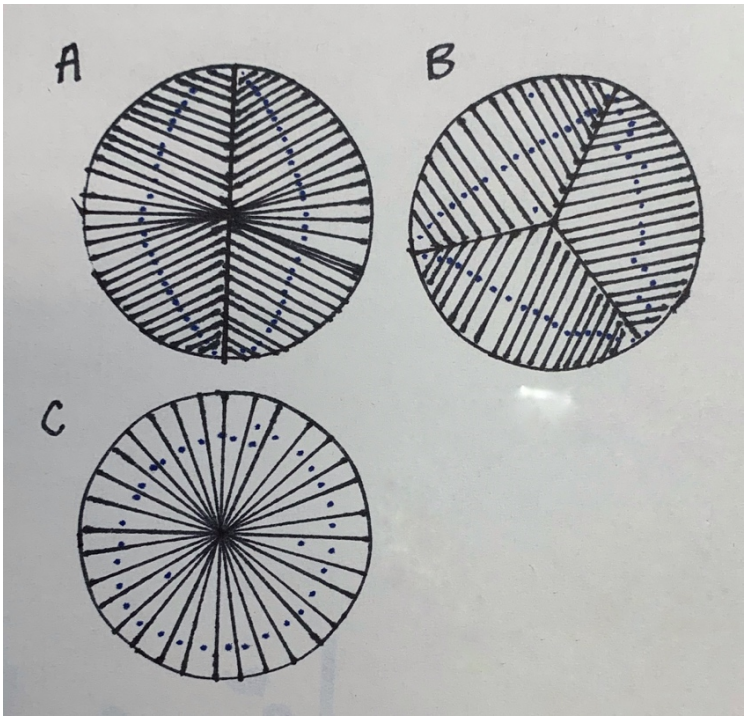

Figure 3: Suture patterns of crystalline lenses. A is mostly found in sharks, rabbits, amphibians, and some teleosts. B is found in humans and most mammals. C is found in some birds, amphibians, and teleosts (drawn by hand after Prince, 1956).

land (Mathis *et al.*, 1988). Vertebrate animals can focus at different distances by changing the shape of the lens (Land, 2005; Somiya & Tamura, 1973), thereby changing the refractive power, or by moving the lens toward and away from the retina.

Human and fish lenses are generally similar in structure, with just a few variations. It is possible for the epithelium of a fish lens to extend beyond its equator towards the posterior side (West *et al.*, 1994). As alluded to above, the human lens is elliptical and of relatively elastic consistency, whereas the fish lens is more spherical and rigid and possesses a higher refractive index (Sivak, 1990; Walls, 1942). In addition, lens accommodation differs between human and fish eyes; humans can use ciliary muscles to change the shape of their lenses, whereas fish typically move their lenses forward and backward, away from and towards the retina, respectively (Somiya & Tamura, 1973).

Moreover, suture patterns vary between humans and teleosts. As lens fibres grow anteriorly and posteriorly, the ends meet and fuse to form a suture. In primates, such as humans and monkeys, the suture is Y-shaped and located on the anterior and posterior side of the lens; by contrast, teleosts, rabbits, and some amphibians have line sutures where the secondary lens fibres meet (Figure 3) (Prince, 1956; Sivak, 1990, 2004).

1.4 PROTEINS OF THE LENS

The crystalline lens is primarily composed of soluble and insoluble proteins. Most of the membrane and cytoskeleton of the lens comprise the insoluble proteins, whereas water-soluble crystallins provide the lens with transparent and refractive properties (Andley, 2007; Oyster, 1999). Water-soluble proteins constitute 90% of the lens and are classified as alpha (α) and beta-gamma (βγ) crystallins. Gamma (γ) crystallins support the transparency and molecular assembly of the lens and are concentrated in the nucleus (Vendra *et al.*, 2016).

α-Crystallins are molecular chaperones (Andley, 2007), which are proteins that can facilitate polypeptide folding. The main functions of these chaperones are to prevent the formation of undesirable structures or disentangling those that do occur (Ellis & Hemmingsen, 1989). Overexpression of these crystallins can confer resistance to thermal and photochemical stress that create undesirable polypeptide structures (Andley, 2007). α-Crystallins can bind to denatured proteins and prevent unwanted aggregation. α-Crystallins were shown to have 60% homology with heat shock proteins (HSPs) (de Jong *et al.*, 1993); their homology HSP 27 confers the ability to protect against thermal aggregation and denaturation (Horwitz, 1992).

βγ-Crystallins mainly operate by affecting lens development, inducing a stress response in the retina, and protecting the retina (Andley, 2007). The center of a vertebrate lens is mainly composed of γ-crystallins. Studies have shown that the nucleus has a higher refractive index than the cortex.

A typical adult rat lens is made up of 41% alpha, 46% beta, and 13% gamma crystallin (Lerman *et al.*, 1966), whereas an adult zebrafish is made up of 7.8% alpha, 36.0% beta, and 47.2 % gamma crystallin (Posner *et al.*, 2008). α-Crystallins and β-crystallins are located mostly in the cortex at lower concentrations, whereas γ -crystallins are most abundant and at the highest concentration in the nucleus for fish lenses (Zhao *et al.*, 2011). Because fish lenses have a higher refractive index than those of land vertebrates, γ-crystallins levels in fish are higher (Sivak, 1978). Teleost crystalline lens proteins are tightly packed and hydrated because of the presence of γM-crystallins (Mahler *et al.*, 2013). In γM-crystallins, the tryptophans (TRPs) are partially lost and replaced with methionine an amino acid with a high refractive index (Mahler *et al.*, 2013). Studies have shown that fish lenses have a higher percentage of methionine content than humans (15% of the total amino acid composition compared with 2.3% in humans). Their habitat may be the cause of the change in methionine because there is less exposure to UV light underwater (Mahler *et al.*, 2013).The replacement of TRP with methionine promotes protein stability, by decreasing the interactions between γM-crystallins and enhancing their solubility. Furthermore, γM-crystallins can achieve a higher refractive power with lower protein concentrations and osmotic pressures (Mahler *et al.*, 2013). Normal γ-crystallins have two domains, each with a TRP pair. The function of TRP is to protect the retina from UV damage by absorbing long wavelengths (Mahler *et al.*,

2013).At least six types of γ-crystallins exist in humans, and many more have been discovered in other species (Vendra *et al.*, 2016).

Human γ-crystallins, namely γC-, γD-, and γS-crystallins, are essential because they contain much more tyrosine, which is the key to the structural stability of the crystalline lens (Vendra *et al.*, 2016). Moreover, γ-crystallins are the only cryoproteins amongst the three crystallins; they are associated with the development of cold-cataracts (Horwitz *et al.*, 1977).

1.5 THE CELL CYCLE OF THE LENS

Generally, the cell cycle of the lens is divided into two phases: interphase and mitosis (M). Various checkpoints regulate the progression of the lens through these stages via cyclin-dependent kinases (CDKs) (Griep, 2006; Johnson & Walker, 1999). CDK can phosphorylate specific substrates to promote DNA synthesis and cell proliferation. Levels of both CDK and cyclin depend on different stages of the cell cycle. Mammalian cells, compared with other eukaryotic cells, have more variations of both CDK and cyclin. This variation allows them to have more control over the cell cycle (Lim & Kaldis, 2013; Morgan, 2007). CDK activity is significant because it ensures that both synthesis (S) and M phase events occur correctly. A few events can either positively or negatively affect CDK activity, such as cyclin binding, phosphorylation, and activation of CDK inhibitors (Johnson & Walker, 1999). Several other checkpoints ensure that no incomplete or damaged chromosomes are replicated or passed on to daughter cells.

Interphase consists of an initial gap phase (G_1), a DNA synthesis (S) phase, and a second gap phase (G_2). The major checkpoints that can delay or allow DNA repair are

G_1/S and G_2/M. Many genes can encode proteins that help with DNA damage repair; for example, p53 is a tumour-suppressing gene that translates into a p53 protein that is able to mediate cell-cycle arrest or apoptosis of the cell (Agarwal *et al.*, 1995; Johnson & Walker, 1999). If repair is possible, the cell determines whether enough growth factors, nutrients, and proteins are present to proceed. If the cell decides to arrest itself, it enters the quiescent G_0 stage, where it can stay for a prolonged period with metabolic activity but no proliferation until the crucial factors are obtained (Cooper, 2000; Johnson & Walker, 1999). From this point forward, the cell has no chance of returning to a previous stage and fixing its DNA. The G_2 checkpoint is where the cell checks the size and amount of protein and whether the DNA has replicated correctly. The final checkpoint is the spindle checkpoint, in which the cell checks whether the sister chromatids are correctly attached to microtubules (Cooper, 2000; Johnson & Walker, 1999).

These checkpoints and regulatory proteins manage the transition between one stage of a cell cycle to another and communicate with extracellular proteins to control cell proliferation (Cooper, 2000; Freeman & Donoghue, 1991). The cell spends 95% of its lifetime in interphase, where it can grow and replicate its DNA. During the G_1 and G_2 phases, the cell grows, organizes the replicated genome, gathers and synthesizes proteins for signalling, and communicates with the external environment to ensure everything is stable and ready for the next step. The M phase, which is composed of mitosis and cytokinesis, contains the crucial steps that utilize microtubules to separate sister chromatids and results in the nuclear division of the cell (Cooper, 2000; Johnson & Walker, 1999). Cytokinesis is the final step, in which the cytoplasm divides and the whole cycle is completed, resulting in two cells that are identical to the parent cell. G_1 is

longer than the G_2 phase because the cells would have to go through increasing in size and stops for a check to see if all the necessary components are ready (Mitchison & Carter, 1975).

A eukaryotic crystalline lens is a desirable option for studying the mechanisms of cell cycles because it continues to grow throughout life and is avascular; it does not require a blood supply to survive (Andley, 2008). Cell proliferation in the germinative zone is an essential mechanism for the lens because it promotes the creation of secondary lens fibres from LECs that comprise the majority of the lens in postnatal organisms; the remainder of the lens is composed of epithelial cells that line the anterior surface (Griep, 2006; Srinivasan & Harding, 1965). The epithelium has three regions that are separated because of their proliferative index, that is, the average number of cells that are dividing. The central epithelium has a slow proliferative rate because most of the cells are dormant, although they do maintain proliferative potential. The active mitotic or germinative zone has a high proliferative index, whereas proliferation is not observed in the cells located in the transition zone located near the equator (Figure 4). The epithelial cells begin to elongate, becoming a secondary lens fibre (Griep, 2006). Each cell changes in morphology during the conversion from an epithelial cell to a lens fibre cell, and because of this phenomenon, they are more suitable for packing (because they are in a hexagonal shape) and maintaining lens transparency.

1.6 Effects of Temperature on Cell Cultures

Most species are categorized as poikilotherms or homeotherms, depending on how they maintain their internal temperature. Homeotherms, including birds and mammals,

maintain a higher body temperature than the environment by elevating their metabolism and burning food (Levesque & Lovegrove, 2014). A healthy human adult has an internal body temperature of 37°C, with slight variations depending on the individual. Species that live in colder environments hibernate for long periods and have a lower body temperature and metabolic rate. Invertebrates are mostly poikilotherms, and three

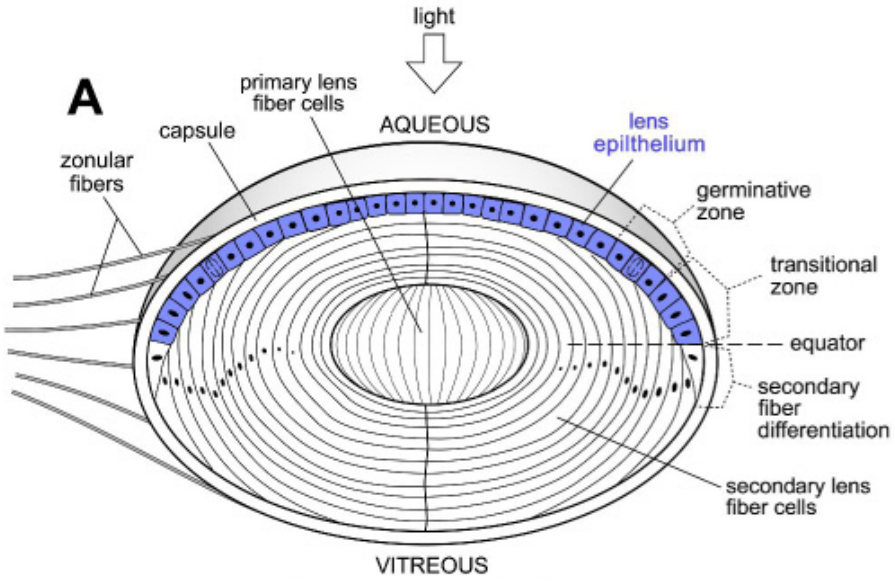

Figure 4: Sagittal cut of the lens. Illustrating different layers and locations of lens epithelial cells as well as their growth zones. The highlighted area represents the location of lens epithelial cells. Reprinted from International Journal of Biochemistry & Cell Biology, 40(3), Andley UP. The lens epithelium: focus on the expression and function of the alpha-crystallin chaperones, 317-23, 2008, with permission from Elsevier.

responses can occur in extreme temperatures: death, quiescence, or hibernation (Block, 1982). Block *et al* (1982) studied species from protozoans to arthropods. He determined that the type of responses that these invertebrate poikilotherms utilize depends on their niche, morphology, and much more (Block, 1982).

Core temperature in mammals is controlled by involuntary (physiological) and voluntary (behavioural) mechanisms (Tan & Knight, 2018). Physiological responses are

autonomic responses that can either dissipate or generate heat, whereas voluntary mechanisms include thermoregulatory behaviours such as seeking warmth and moving into or out of shade. Brown adipose tissue is a thermogenic tissue that provides heat to smaller animals when they are in cold environments and is an example of physiology used as a voluntary mechanism. Brown adipose tissue is activated by the sympathetic nervous system and can convert chemical energy into heat (Betz & Enerback, 2015). Other physiological effects induced by involuntary mechanisms include vasoconstriction, shivering, and water evaporation. These are classed as physiological responses and are coordinated by the peripheral and central thermoreceptors (Rastogi, 2007; Tan & Knight, 2018). A central thermoreceptor is situated in the hypothalamus, whereas peripheral thermoreceptors are found in the skin and can transmit information to the hypothalamus. The anterior and posterior hypothalamic nuclei are the main nuclei associated with temperature (Nolte, 2016). The anterior hypothalamic center, or heat center, is activated by warmth and can initiate heat loss through the production of sweat, whereas the posterior hypothalamic center is triggered by cold conditions and can generate heat and preservation responses, such as shivering and vasoconstriction of the skin (Rastogi, 2007).

Organisms that live in warmer environments are not required to consume as much food as those in colder environments; the surrounding temperature, which is similar to the animal's core temperature, is sufficient to keep the animal alive. Heat is conserved in colder environments and lost in warmer ones (Rastogi, 2007).

Fish are aquatic poikilotherms with body temperatures that vary with the surrounding environment (Rastogi, 2007). They use gills as their main respiratory exchange organ because they have a higher surface area for the movement of oxygen into

the body and waste out of the body. A counter-current mechanism maintains the core temperature of fish very close to the temperature of the water, even with the heat created by muscular activity (Rastogi, 2007).

Terrestrial poikilotherms face a more significant problem depending on their niche, because of environmental temperature fluctuations. For example, a species living in the desert faces extreme temperatures of 50°C during the day and 10°C at night. Usually, species living in such environments regulate their internal temperature by adjusting their behaviours and utilizing internal acclimatization (Rastogi, 2007). Acclimatization is a reversible long-term physiological response that causes an organism to slowly adapt to the environment (Speakman, 2001). Acclimatization due to high or low temperatures can result in a change in blood ionic concentrations, which can have a considerable influence on the metabolism of cells; that is, protein synthesis (Rao, 1963).

Studies have shown an ocular temperature gradient that varies across the orbit of the eye depending on the ambient temperature and whether the eyelid is open or closed (Voaden, 1971). The molecular organization of the protein of the ocular lens is crucial to its transparency (Andley, 2008); therefore, any alteration in the environment may cause obscurity to the clarity of the lens and lead to difficulties with vision. For example, in rat ocular lenses, if the ambient temperature falls below 37°C, lens opacification is observed (Hikida & Iwata, 1985). If the ambient temperature is 23°C, the human ocular temperature is 34.8°C (Rosenbluth & Fatt, 1977). Clinical observations and experiments have noted that prolonged exposure to higher temperatures leads to transparency changes (more opacification) in ocular lenses, which affect their elasticity and transparency (Al-Ghadyan & Cotlier, 1986; Sharon *et al.*, 2008). Thermal cataracts have been observed in

furnace workers, bakers, glass industry workers, and even in individuals who live in hot countries (Vos & van Norren, 2004). This type of cataract is an occupational condition that is associated with an indirect increased exposure of the crystalline lens to light energy (Vos & van Norren, 2004). Research has suggested that many components can raise the temperature of both the posterior chamber and lens, such as a rise in ambient temperature, exposure to UV light, or severe dehydration in the body (Al-Ghadyan & Cotlier, 1986). Rises in temperature are caused by the pigmented epithelium of the iris absorbing heat combined with an increase in temperature from the environment, which can cause the temperature of the aqueous humour in the posterior chamber and lens to rise (Al-Ghadyan & Cotlier, 1986). Fish are also susceptible to cataracts; cataracts are observed when the temperature of the lens increases to 37°C and above (Iwata, 1985). Impaired vision has detrimental consequences for fish that live above the twilight zone because they require sight to hunt (Noga *et al.*, 1981).

The crystalline lens cell membrane content can also help fish adapt to colder temperatures. Lens membranes contain cholesterol, phospholipids, and fatty acids. Iwata (1985) found that the rainbow trout crystalline lens has a lower ratio of cholesterol to phospholipids compared with the bovine crystalline lens: 1.02 and 1.48, respectively. Meyer-Rochow *et al* (1979) experimented with Antarctic fish and found large amounts of polyunsaturated fatty acids in the ocular lenses of *T. Borchgrevinki* and *T. Bernacchii*. These fish live in the Antarctic environment at very low temperatures (Meyer-Rochow & Pyle, 1980). Iwata *et al* (1985) also confirmed that a larger number of unsaturated fatty acids in the ocular lenses of rainbow trout compared with bovine ocular lenses (Hikida & Iwata, 1985). Therefore, these fish should have biochemical and physiological

adaptations to low temperatures. As the ratio of cholesterol to phospholipids in rainbow trout lenses is smaller than that of bovine lenses, it may be postulated that rainbow trout are more resistant to the cold. Cholesterol can harden the cell membrane when temperatures increase and loosen it when temperatures decrease (Iwata, 1985).

II. INTRODUCTION

The crystalline lens is a transparent, biconcave, and elastic structure that helps to refract and focus light on to the retina. In terrestrial animals, the lens contributes about 1/3 of the power of the eye for distant objects. The cornea, a transparent protective outer layer of the eye, contributes to the rest of the power of these eyes. In aquatic animals, corneal power is neutralized by water because the refractive indices of the cornea and water are similar, therefore the lens is wholly responsible for the refractive power of the eye. The loss of corneal power is compensated by a higher refractive index in the lens. A mammalian lens has an equivalent refractive index of a lens is 1.38 – 1.48, whereas a fish lens can have an index of refraction of 1.41 – 1.55 (Michael & Brismar, 2001; Mutti *et al.*, 1995; Pierscionek & Augusteyn, 1995).

The growth of the lens happens throughout life by adding new fibres to the old. The rate of growth is the highest during infancy and childhood, and as age increases, the growth rate decreases (Pokorny *et al.*, 1987). An increase in age can bring about age-related cataracts which is the world's second leading cause of blindness (WHO, 2018). Cataracts is the opacification of the lens where it blocks the passage of light, thereby unable to create an image. Besides age, cataracts can be caused by ultraviolet radiation, diabetes, family history, trauma, and temperature (Dolin, 1994; Francois, 1982; Oriowo *et al.*, 1997; Pollreisz & Schmidt-Erfurth, 2010; Roper-Hall, 1977). Heat-related cataracts could be seen when lenses are exposed to 40^{o}C for at least 6 hours (Sharon *et al.*, 2008). Workers in high temperature industries like glass, molten metal, and bakeries have a higher incidence of cataracts compared to other occupations (Lydahl & Philipson,

1984). Cold cataracts can also be observed in mammals whose lenses develop cataracts when they are exposed to temperatures below their optimal physiological levels (Bermudez *et al.*, 2011).

Crystallins are proteins in the crystalline lens that confer refractive properties to the lens. All vertebrate lenses contain α- and β-crystallins, and often a third major crystallin, depending on the species. Mammalian and teleost fish lenses also contain γ-crystallins, while δ-crystallins are found in avian and reptilian lenses. Many crystallins have additional non-refractive functions; α-crystallins act as heat shock proteins, protecting lenses from denaturation arising from heat, and γ-crystallins are thought to be cryoproteins, protecting lenses from the cold. In mammalian lenses, the concentration of α-crystallins is higher than in teleost lenses, while the opposite is true for γ-crystallins, suggesting that mammalian lenses would be better protected in warmer conditions and teleost lenses better protected in colder temperature (Ahrend *et al.*, 1987; de Jong *et al.*, 1993; Lerman *et al.*, 1966; Mahler *et al.*, 2013).

All cells within the lens start out as epithelial cells, which either retain their epithelial cell properties, or differentiate into lens fibre cells. Because the eyes of all vertebrate species share the same basic embryology, this study was undertaken to determine whether temperature differences affect the behaviour of lens epithelial cells derived from human and fish lenses. The proliferation indices of these cells grown in culture were used to assess changes in cellular behaviour.

III. METHODS AND MATERIALS

3.1 CELL CULTURE

3.1.1 Preparation from frozen stocks

Human LECs were retrieved from their storage in liquid nitrogen where they had been kept frozen (ATCC CRL-11421). The cells were rapidly defrosted into a slushy consistency and immediately placed into a vial with 5 ml of DMEM: Nutrient Mixture F-12 (DMEM/F12; Fisher Scientific, 21041025), containing 15% FBS (Fisher Scientific, 12484028) and 1% pen-strep (Fisher Scientific, 15140122). The medium was brought to room temperature each time before adding it to the culture. This was done because human LECs are heat sensitive (Wise, 2002), and furthermore, if the cells were cold-shocked, phenotypical modifications would be induced, thereby leading to a reduction in metabolism, cell-cycle arrest, activation of apoptosis, or even disassembly of the cytoskeleton (Neutelings *et al.*, 2013). Depending on the size of the culture flasks or dishes, different seeding densities and volumes of growth medium were added according to the numbers provided by Thermofisher. For example, in T-25 flasks, the seeding density was 7×10^5 cells/ml using 3–5 ml of medium (Table 1, T-25 flask volumes; ThermoFisher Scientific Inc., 2010). The culture flasks were then incubated at 37°C with 5% CO_2 until 80–90% confluence had been reached. The cells were observed daily to check for any fungal contamination or other abnormalities. Human LECs are less resistant to experimental trauma; therefore, decontaminating the flow hood, external surfaces of medium bottles, pipettes, and gloves with 70% ethanol was crucial (Geeraets, 1972).

Table 1: List of numbers for cell culture. These are numbers that were retrieved from Thermofisher to use as a reference. Various dishes and sizes were included and many handy numbers like surface area and etc. Using these numbers and their pattern, I determined that the surface area is 1.25 X smaller than the actual dish area. On average, there were **$3.6 \text{ X } 10^4$ Cells/ml**. By having these two as a guideline, I was able to determine that the 14 mm dish requires around **$4 \text{ X } 10^4$ to $5 \text{ X } 10^4$ Cells/ml**. To be on the safer side, I utilized **to $5 \text{ X } 10^4$ Cells/ml** as my seeding density.

		Surface area (mm^2)	Seeding density (Cells/ml)	Cells at confluency (Cells/ml)	Versene (ml of 0.53 mm EDTA)	Trypsin (ml of 0.05% trypsin, 0.53mm EDTA)	Growth medium (ml)
Dishes	35 mm	962	$0.3 \text{ X } 10^6$	$1.2 \text{ X } 10^6$	1	1	2
	60 mm	2,827	$0.8 \text{ X } 10^6$	$3.2 \text{ X } 10^6$	3	2	3
	100 mm	7,854	$2.2 \text{ X } 10^6$	$8.8 \text{ X } 10^6$	5	3	10
	150 mm	17,671	$5.0 \text{ X } 10^6$	$20.0 \text{ X } 10^6$	10	8	20
Cluster plates	6-well	962	$0.3 \text{ X } 10^6$	$1.2 \text{ X } 10^6$	2	2	3 - 5
	12-well	401	$0.1 \text{ X } 10^6$	$0.4 \text{ X } 10^6$	1	1	1 - 2
	24-well	200	$0.05 \text{ X } 10^6$	$0.2 \text{ X } 10^6$	0.5	0.5	0.5 – 1.0
Flasks	T-25	2,500	$0.7 \text{ X } 10^6$	$2.8 \text{ X } 10^6$	3	3	3 - 5
	T-75	6,500	$2.1 \text{ X } 10^6$	$8.4 \text{ X } 10^6$	5	5	8 - 15
	T-160	16,000	$4.6 \text{ X } 10^6$	$18.4 \text{ X } 10^6$	10	10	15 - 30

This table was based on HeLa cells (ThermoFisher Scientific Inc., 2010).

Fish LECs (gift from N. Bols), isolated from rainbow trout, were rapidly defrosted into a slushy consistency, and then immediately placed into a vial with 10 ml of culture medium. The culture medium for fish cells was different to that used for human cells. Hyclone™ Leibovitz L-15 medium (Fisher Scientific SH3052501) was used as the base medium and supplemented with 15% FBS and 1% pen-strep. The fish LECs were seeded into flasks using the same seeding density provided by Thermofisher, cultured at room temperature with no extra CO_2 required (Hamilton *et al.*, 2018). Because fish cells do not require incubation when plated into dishes or T-25/75 flasks with a ventilation cap, the culture vessel was sealed with parafilm to optimize sterility and minimize the risk of contamination.

3.1.2 Seeding of lens epithelial cell cultures

Human and fish LECs grow at optimal temperatures of 37ºC and between 15 – 20ºC, respectively. The average of the range, 18°C, was chosen to be the optimal temperature for fish LECs. A temperature change of ± 5ºC was selected to test higher and lower temperature effects; for fish LECs, the ± 5°C changes were set relative to the limits of the range of temperature that rainbow trout prefers. Therefore, human LECs were incubated in 42ºC, 37ºC, and 32ºC with 5% CO_2, whereas fish LECs were incubated in 10ºC (refrigerator), 18ºC (room temperature), and 25ºC (incubator) without 5% CO_2.

Human and fish cells were seeded on the same day at a density of 5×10^4 cells/ml (determined in Table 1, calculated for 14-mm surface area; Figure 5) with 200 μL of the same culture media used for preparing the human and fish stocks, respectively, onto 35 mm glass-bottom microwell dishes (MatTek Corp., Ashland, MA P35GCOL-1.0-

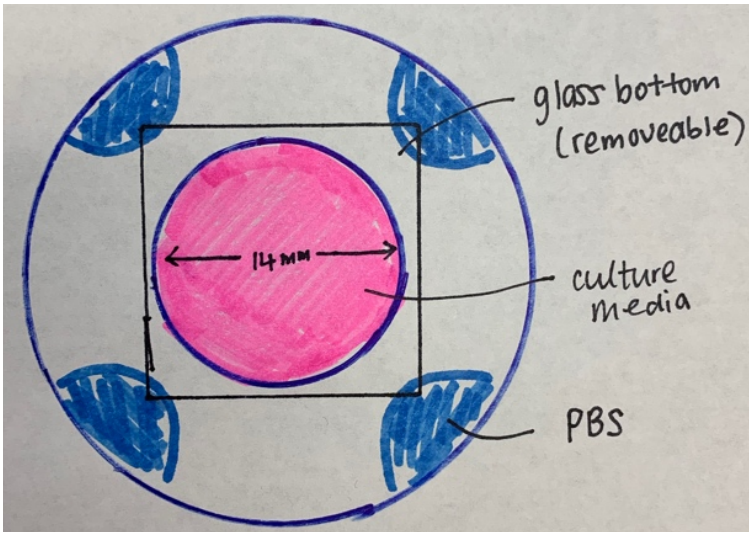

Figure 5: Representation of a cultured glass bottom petri dish. The black box represents the coverslip, removable using a sharp blade. The culture was seeded in the 14-mm-diameter circle (pink shaded area) with PBS (blue) in the corners, providing moisture. The picture was drawn and not to scale.

14-C). Furthermore, four replicates were performed for each temperature and species to allow the variability associated with any phenomenon to be statistically analyzed. Cell cultures were analyzed 1, 2, 4, 6, 8, and 12 days post- seeding (dps). Three hours prior to fixation, 0.2 µL of 5-ethynyl-2'-deoxyuridine (EdU), was added to each culture plate to mark proliferating cells.

3.2 Fixation and Immunohistochemistry of Cells

The media were removed, and the cells were fixed by adding 200 μL of 4% (w/v) paraformaldehyde (PFA) in PBS to each plate for 10 min. The cells were washed (3x 5 min) with PBS, and then permeabilized with 200 μL of 0.1% Triton X-100 (15min). Cultures were washed again with PBS (3x5min).

To label cells that had incorporated EdU, an EdU iFluor 488 staining proliferation kit (abcam 219801) was used, following manufacturer instructions except for volumes

used. The EdU reaction mixture was created using 86 μL of TBS, 4 μL of $CuSO_4$, 0.24 μL of iFluor 488 azide, and 10 μL of 1X EdU additive solution per test. Kimwipes® delicate task wipers were soaked in distilled water and placed in the incubator to maintain the moisture necessary to prevent the cells from drying out. Each plate was incubated in a dark box for 30 min. The cells were then washed (3X) with wash buffer (3% BSA in PBS) and once with PBS. Coverslips from the wells were then carefully detached and a subset of cultures were labelled for tight junctions (zonular occludens-1; ZO-1). A subset of cells were first stained with ZO-1 mouse monoclonal antibody (ZO-1A12, Fisher #33-9100; 2 μg/ml in 2% BSA, overnight at 4°C) then washed (3X5 min PBS) before being incubated with a goat anti-mouse IgG (H+L) f(ab) specific tetramethylrhodamine (TRITC) antibody (Sigma-Aldrich #T6653; 5 μg/ml in 2% BSA, 1 h, 37°C), followed by 3X5 min PBS wash. All cell cultures were labelled for 15 min in 100 μL of 4′,6-diamidino-2-phenylindole (DAPI; 1μg/mL, Molecular Probes, D1306) and washed in PBS (3x5min), before mounting on a slide with Prolong Gold Antifade (Sigma, P36930) or coverslips were directly mounted onto slides using Fluoroshield Mounting Medium with DAPI (abcam, ab104139)

3.3 Data Collection and Analysis

Slides were examined under a Zeiss Deconvolution Microscope (Carl Zeiss Axio Imager Z-2 with Axiocam MRC5, Germany under 20x magnification (Plan Apochromat 20X /0.8 420650-9901), using the AxioVision software. Cells were imaged using the FITC and DAPI filter sets, to capture emission wavelengths of 525 nm (EdU) and 461 nm (DAPI), respectively. Three regions (1150 µm x 850 µm) were analysed per slide and

processed for numbers of proliferating cells, total number of cells and changes in distributions as a function of temperature.

3.3.1 Proliferation index

The obtained images were then imported into Fiji is Just Image J (FIJI) (https://fiji.sc/). First, the scale was set to enable FIJI to provide an accurate scale bar and area (0.1668 mm/1 pixel). Next, images were modified with the following steps: process, subtract background, and set the rolling ball radius to 150 pixels (radius of curvature). By this point, the image was clear enough to count the cells, and therefore a plugin (https://forum.image.sc/t/randomized-rois/6093) was used to find 10 random regions of interest (ROIs) 50 µm x 50 µm in size. The steps for this were as follows: click on plugins, then on macroinstruction (macro), and install the random ROI. The macro was found on the ImageJ question form listed by G. Landini (at www.bham.ac.uk) as a Random Sample and Measure macro. It was possible to customize how many random areas were selected or how large the desired area should be. All the cells in each ROI were counted, including those touching the barriers of the ROI. Ten non-overlapping ROIs were selected per image (Figure 6). The cells, even those that touched the barrier, were manually counted.

Each ROI is 2,500 μm^2, covering an area of 25,000 μm^2 because there are 10. This value was then multiplied by 3 because there were three non-overlapping images taken per replicate, yielding 75,000 μm^2 per replicate. There were four replicates (n=4) done for each experimental time point (6 time points), temperature (3 temperatures) and species (2 species). All the DAPI, EdU and ZO-1-stained cells across the ROIs for each

replicate (per time point per temperature per species) were summed to give the best representation of the total number of cells, number of proliferating cells and the proliferation index, calculated as the percentage of proliferating cells divided by the total of cells.

3.3.2 Distribution patterns

Nearest neighbour analysis (NNA) can show the settlement patterns of cells by calculating the distance between each cell. The values range from 0 to 2.15, with 0 representing clustered distributions, 1 representing random distribution and 2.15 representing highly regular distributions. For each of the three 1150 µm x 850 µm images collected, the nearest neighbour value (R_n) was calculated using the following equation:

$$R_n = \frac{\overline{D}(Obs)}{(0.5)\left(\sqrt{\frac{a}{n}}\right)}$$

where $\overline{D}(Obs)$ is the average of all observed nearest distance values, a is the area of interest, and n is the total number of cells counted.

The positions of the cells were determined using a program (https://forum.image.sc/t/the-center-of-cells/5531/8) that could create centroids and could find the centre of each cell. Each cell's (x,y) coordinates were used to determine the nearest neighbour values, which gave an idea of the distribution patterns, i.e., whether cells were uniformly organized, randomly organized, or clumped.

3.3.3 Statistical Analyses

All data were analyzed using mixed model analysis of variance (ANOVA) tests, with

time and temperature as factors (Statistica 8, Dell Software). Bonferroni corrected t-tests were used Tukey's Significant Difference (HSD) post-hoc tests were used to determine

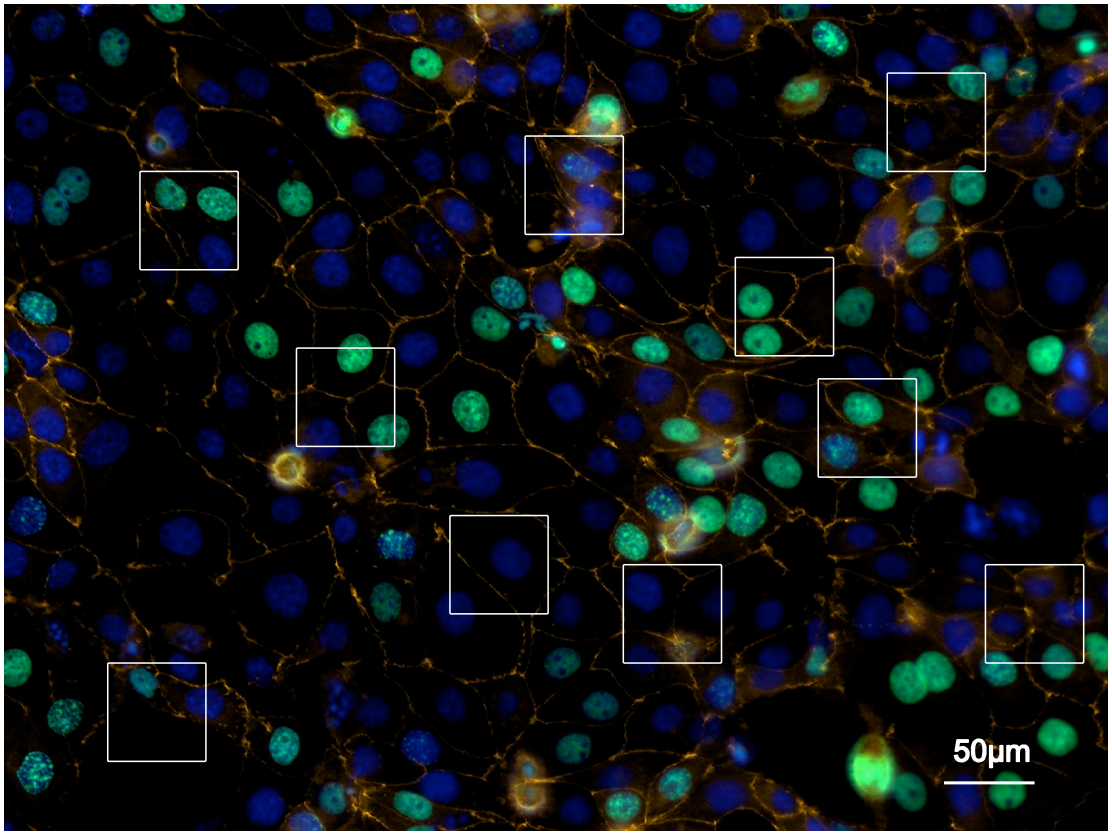

Figure 6: Human LECs labelled for mitotic cells (green), non-mitotic cells (blue) and tight juncions (orange lines). Random regions of interests (ROIs; white squares) were selected by macro and cells, outlined in orange, were traced three times.

any differences temperatures and Bonferr time point (dps), and species. For all experiments, differences were considered significant if $P \leq 0.05$. All means are reported with the standard error unless otherwise stated.

IV. RESULTS

4.1 EFFECTS OF TEMPERATURE AND TOTAL NUMBER OF CELLS

4.1.1 Growth of human LECs at various temperatures

The total number of cells, number of mitotic cells, and proliferation indices were calculated and graphed using the number of DAPI-stained, EdU-stained cells (human: Figure 7; fish: Figure 8), and number of DAPI divided by number of EdU-stained cells, respectively. The overall total number of cells grown at optimal temperatures (mean across all time points ± SEM: 78.5 ± 5.3) was significantly greater than those grown at both the lowest (57.5 ± 5.2; $P = 0.002$) and highest (15.8 ± 2.1; $P < 0.001$) temperatures, with LEC growth at the lowest temperature better than at the highest temperature ($P < 0.001$; Figure 9). However, there was no interaction between the temperature and time post-seeding ($P = 0.062$), indicating that the total number of cells as a function of time for each temperature was similar across the twelve days of experimentation.

When comparing the overall number of replicating cells as a function of temperature, the LECs grown at the optimal temperature (33.1 ± 3.0) was significantly higher than those grown at both the lowest (23.5 ± 2.5; $P = 0.008$) and highest (4.4 ± 0.9; $P = 0.002$) temperatures. Again, the number of proliferating cells was greater for those grown at the lowest temperature compared to those at the highest temperature ($P < 0.001$; Figure 9B). The change in mitotic numbers as a function of time was also analogous to the total number of cells across twelve days, where temperature had no effect on the number of mitotic cells across the experimental time points ($P = 0.134$). Comparison of the overall proliferation indices indicated that human LECs grown at the highest

temperatures (26.8 ± 3.4%) showed a lower proliferation index compared to those grown at optimal (41.9 ± 2.3%; P = 0.017) and lowest temperatures (41.5 ± 2.2%; P = 0.020; Figure 9 inset).

4.1.2 Growth of fish LECs at various temperatures

There was no pronounced pattern to the total number of cells across the three temperatures for fish LECs (Figure 11A). However, in contrast to the human LECs, the overall number of cells for fish LECs were greater for the highest temperature (68.8 ± 4.3) compared to the optimal temperature (45.5 ± 5.5; P = 0.003). The number of cells in the highest temperature group was also greater than those grown at the lowest temperature (46.8 ± 6.7; P = 0.004). No differences were found between the cultures growing at the optimal and the lowest temperatures (P = 0.966).

Similar to the human LECs, the overall number of mitotic cells in the fish LECs was highest in the optimal group (9.5 ± 1.7) compared to the lowest (2.9 ± 1.0; P < 0.001) and highest (P < 0.001) temperatures, the latter of which never showed any mitotic cells in any of the cultures (Figure 11B). However, unlike human LECs, temperature did affect the growth of the cells as a function of time (P < 0.001). Proliferation appeared to be cyclical in the fish LECs grown at the optimal temperature; initially, cultures did not have any mitotic cells, but a sudden significant increase was observed after 2 dps (13.5 ± 4.4; P = 0.001). A gradual decrease in cell numbers followed between 4 to 8 dps (from 11.3 ± 2.8 down to 3.5 ± 0.9 cells), but a second significant increase occurred between 8 and 12 dps (P <0.001), with the number of mitotic cells reaching 21.3 ± 1.8. Fish LECs grown at the lowest temperature also initially showed no mitotic activity followed by an

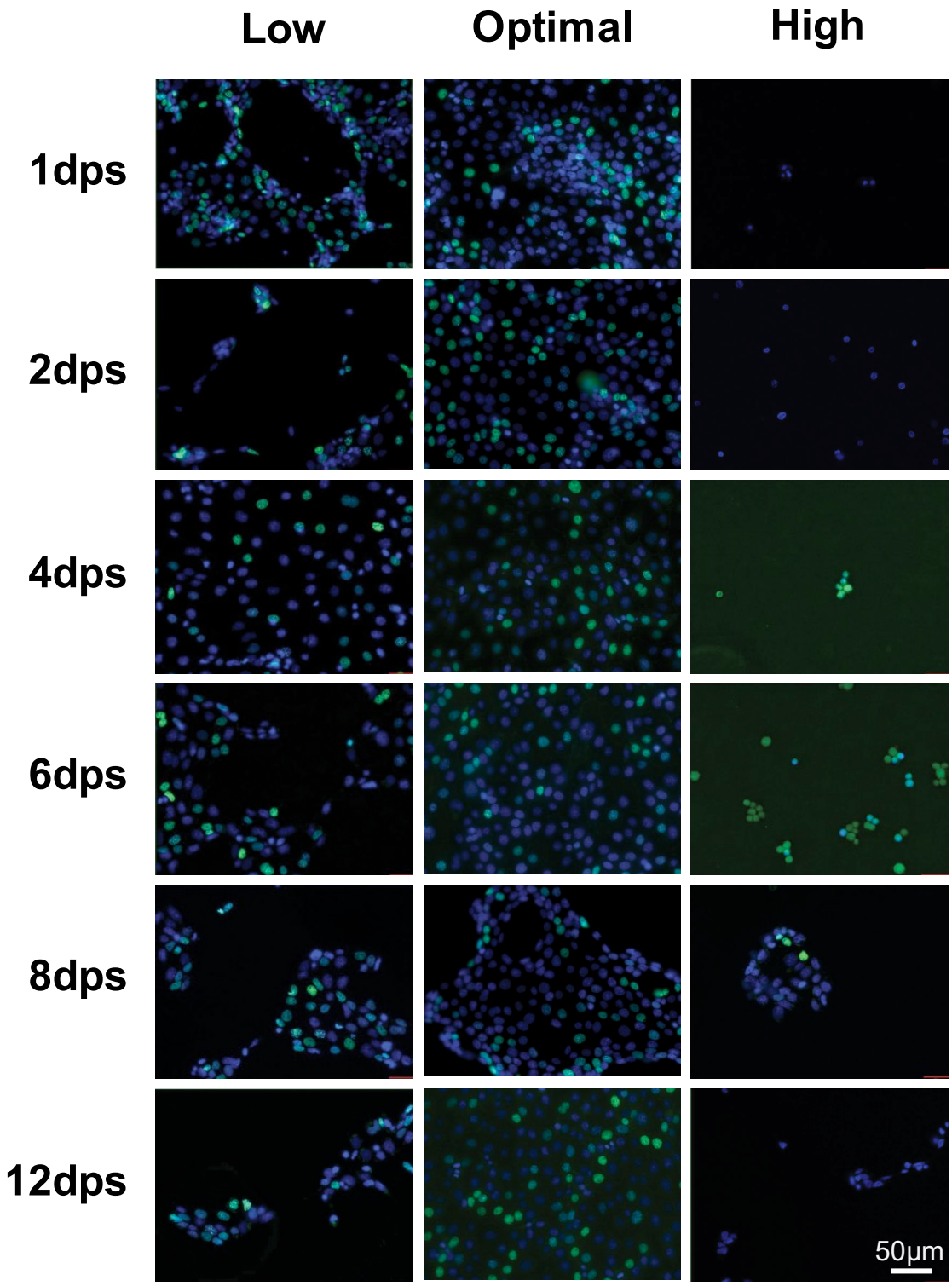

Figure 7: Micrographs of human LECs at various temperatures. All nuclei were stained with DAPI (blue). Mitotic ells are shown in green. Scale bar = 50 µm

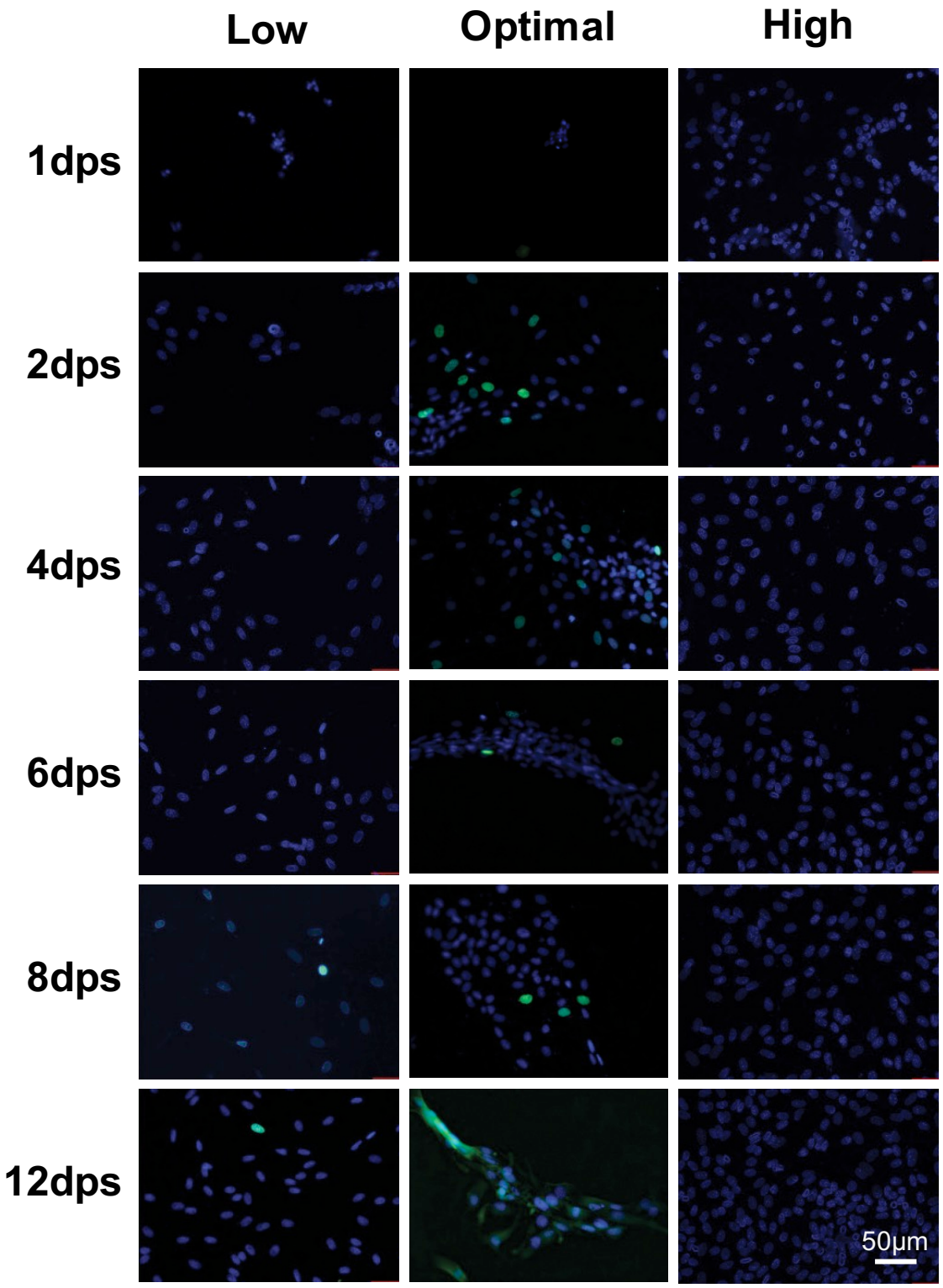

Figure 8: Micrographs showing fish LECs at various temperatures. All nuclei were stained with DAPI (blue). Mitotic ells are shown in green. Scale bar = 50 µm

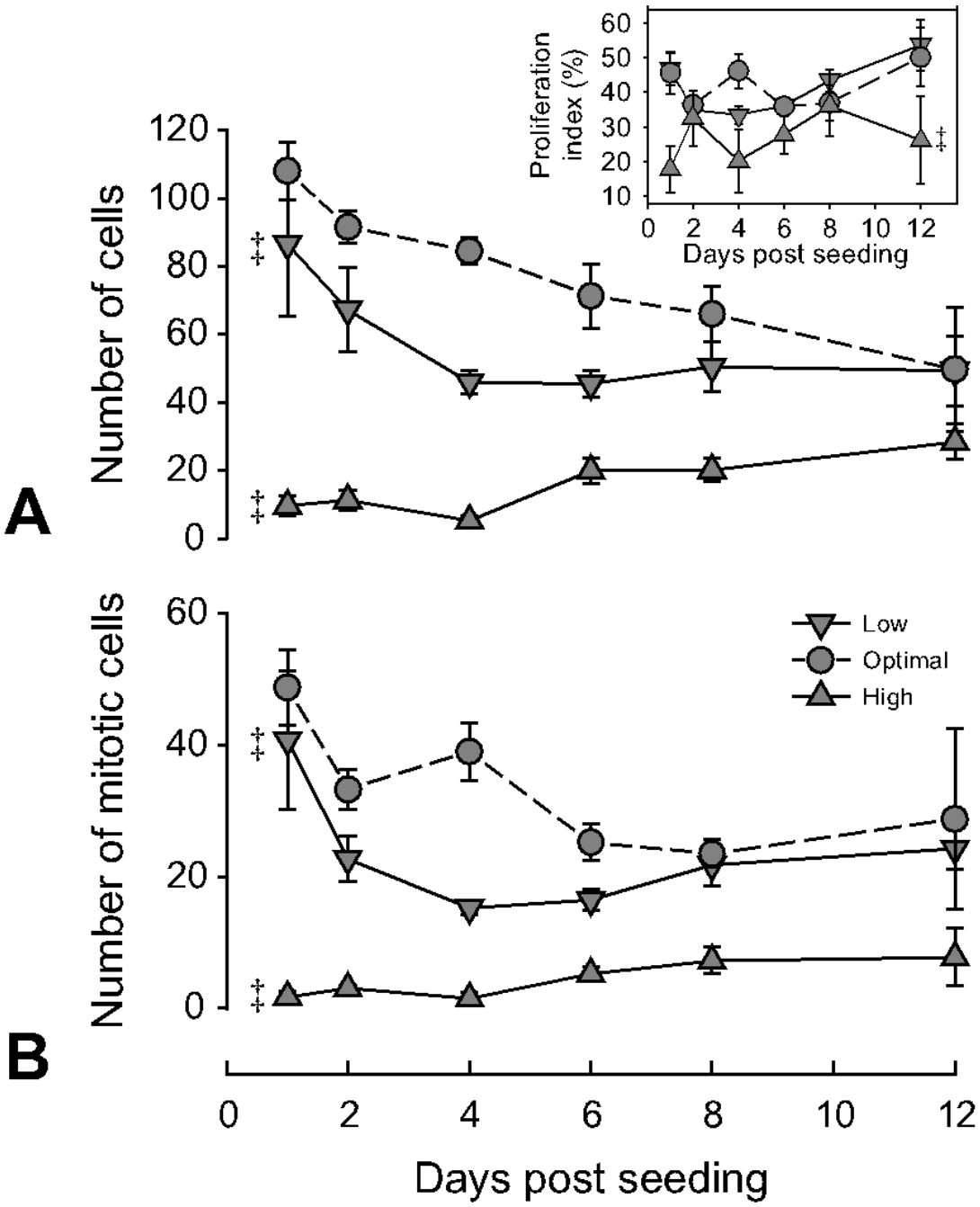

Figure 9: Growth profile of human LECs consisting of the total number of cells (A) and number of mitotic cells (B). Cultures grown at the optimal temperature showed a higher number of cells and a higher number of mitotic cells than those grown at non-optimal temperatures. **Inset:** Proliferation index showing the percentage of mitotic cells. Overall, the index for the cultures grown at the highest temperature was lower than those grown at both the optimal temperature and lowest temperatures. Double daggers (‡) represent overall differences from those grown at the optimal temperature across the entire time course.

increase in mitosis; however, the increase was much more gradual, with significantly higher numbers (10.3 ± 3.6) at 12 dps. The proliferation index for fish LECs followed the same graphical pattern as the number of mitotic cells for fish LECs, where the optimal temperature group had the highest proliferation (25.0 ± 5.5%), followed by those grown at the lowest temperature (11.5 ± 4.7%; Figure 11 inset). Given that there were no mitotic cells in the fish LECs grown at the highest temperature, the proliferation index for this group was 0. The proliferation index for the optimal temperature group was significantly greater than those grown at the lowest ($P = 0.002$) and highest temperatures ($P < 0.001$), while those at the lowest temperature showed a greater proliferation index than the highest group ($P = 0.007$).

4.2 EFFECT OF TEMPERATURE ON CELL DISTRIBUTION

4.2.1 Morphology of confluent cultures

When confluent, human LECs appeared to be a monolayer of simple polygonal cells. The cells did not overlap with one another or clump together. Tight junctions-staining was obvious, indicating typical epithelial cell morphology (Figure 10A). In contrast, fish

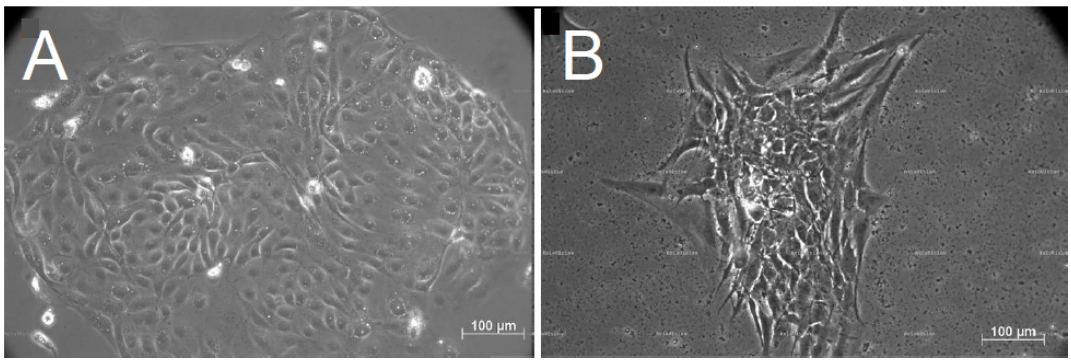

Figure 10: Initial cell morphologies for human (A) and fish (B) LECs. Human LECs are flatter, able to cover more space, and are in few layers. In contrast, fish LECs grew in clumps (B). The human cell body to cytoplasm ratio is smaller. Scale bar represents 100 μm.

LECs resembled stratified fibroblasts and formed clusters in the cultures (Figure 10B). TJ-staining in fish LECs were punctate and sparse.

4.2.2 Effect of temperature on cell size

The area and perimeter of human LECs at 1 dps for the highest temperature group (area: 7.4 ± 0.3 mm²; perimeter: 8.5 ± 0.1 mm) was very much smaller than for the optimal temperature (area: 20.6 ± 0.5 mm²; perimeter: 16.9 ± 0.1 mm; Figure 12). However, the change in area and perimeter for the optimal temperature group did not change as greatly over time (Δ 1 – 12 dps: 1.4 ± 0.3 ± mm² and 1.6 ± 0.1 mm, respectively) was much smaller than for the highest temperature group (Δ 1 – 12 dps: 14.4 ± 0.3 mm² and 8.5 ± 0.2 mm, respectively). The lowest temperature group also did not change greatly (Δ 1 – 12 dps: 0.3 ± 1.0 mm² and 2.1 ± 0.1 mm, for area and perimeter respectively).

In contrast, fish LECs showed temperature-dependent patterns for area that differed from those for the perimeter, and neither was similar to the patterns of the human LECs (Figure 13). Like the human LECs, areas for fish LECs grown at the optimal temperature were greatest (average across all time points: 22.2 ± 0.1 mm²), but did not vary much from 1 to 12 dps (Δ 1 – 12 dps: 0.4 ± 0.2 mm²). However, for this species, the lowest temperature group showed the smallest area at 1 dps (4.9 ± 0.1 mm²) but the change from 1 dps to 12 dps was much greater (Δ 1 - 12 dps: 14.4 ± 0.1 mm²). The area for the highest temperature was also stable, and did not change greatly (Δ 1 – 12 dps: 0.1 ± 0.1 mm²). The perimeter for the highest temperature group was the greatest and also did not vary greatly (average across all time points: 20.5 ± 0.1 mm; Δ 1 – 12 dps: 0.2 ± 0.1 mm). The optimal temperature showed slightly smaller perimeters (across all time

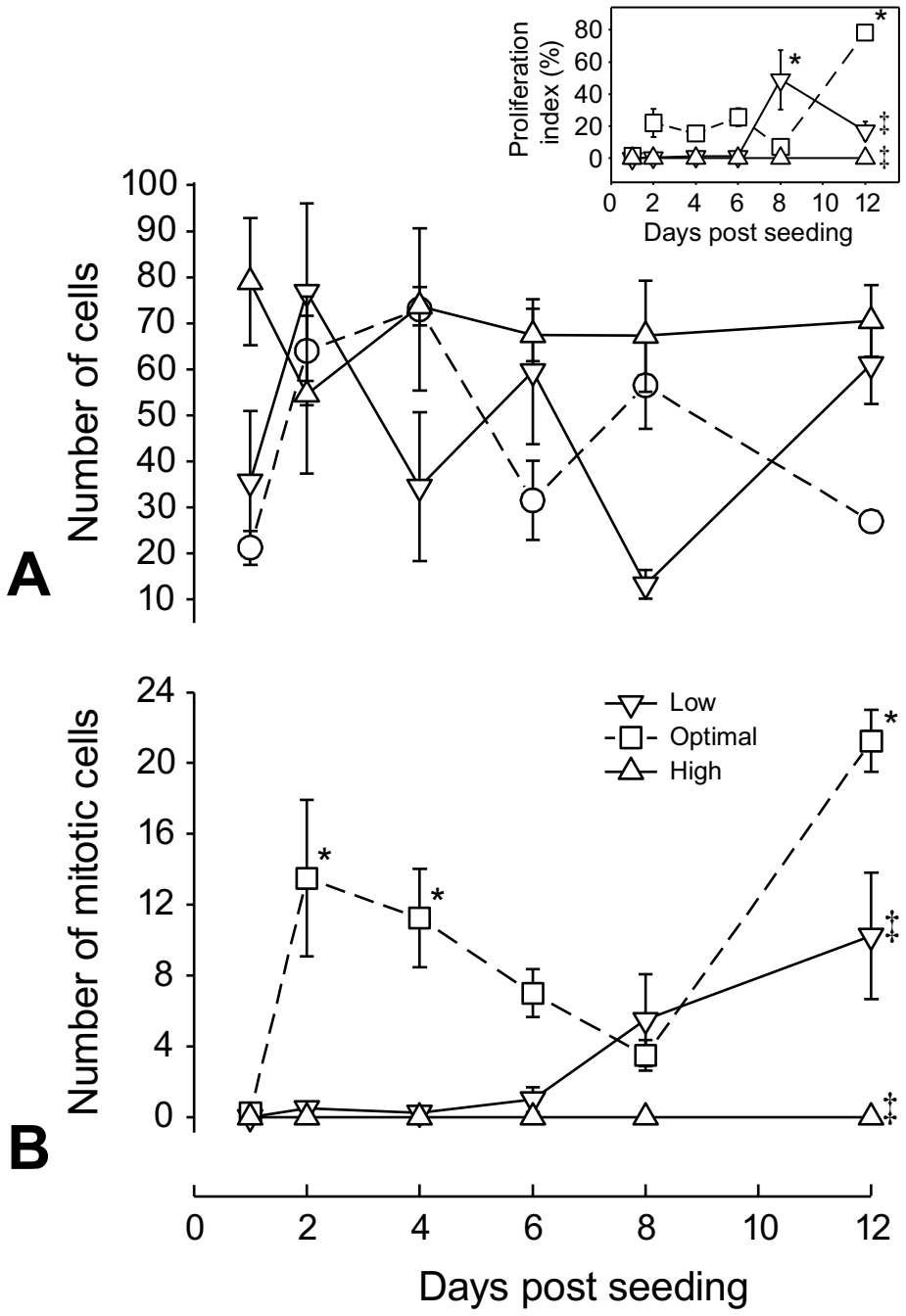

Figure 11: Growth profile of fish LECs consisting of the total number of cells (A) and number of mitotic cells (B). Cultures grown at the highest temperature showed the greatest number of cells compared to optimal and low temperatures. When grown at optimal temperature, the cultures showed a higher number of mitotic cells than those grown at non-optimal temperatures. **Inset:** Proliferation index showing the percentage of mitotic cells. Overall, the index for the cultures grown at the optimal temperature was greater than those grown at both the lowest and highest temperatures. Double daggers (‡) represent overall differences from those grown at the optimal temperature across the entire time course. Asterisks (*) represent the differences from those grown at 1dps per temperatures.

points: 19.5 ± 0.1 mm) and again, did not vary from 1 dps to 12 dps (Δ: 0.1 ± 0.2 mm).

For fish LECs, the perimeter for the lowest temperature group was smallest at 1 dps (8.1 ± 0.2 mm), but showed the greatest increase across the time period (Δ 1 – 12 dps: 13.0 ± 0.2 mm).

4.3.3 Effect of temperature on clumping

Nearest neighbour analyses indicated that human LECs grown at the optimal temperature did not show changes in clumping over time. The cells remained in a randomly scattered distribution (average across all time points: Rn = 0.99 ± 0.05; Figure 14A). However, cells were initially clumped at 1 dps when grown at the two non-optimal temperatures (lowest: 0.26 ± 0.05, highest: 0.38 ± 0.04), with both groups showing a brief change towards a random distribution at 4 dps (lowest: 0.89 ± 0.04, highest: 0.63 ± 0.04). Distributions reverted back to clumped, starting at 6 dps. In contrast, fish LECs were initially randomly distributed at 1 dps (R_n = 0.76 ± 0.02; Figure 14B), but gradually became more clumped, across the experimental time course. The distribution was most clumped at 8 dps (R_n = 0.24 ± 0.04). However, fish LECs behaved in an opposite manner to human LECs at non-optimal temperatures. At the lowest temperature, the distribution was initially clumped (1 dps: R_n = 0.14 ± 0.04), and grew towards a random distribution, stabilizing at 6 dps (R_n = 1.00 ± 0.02), whereas the highest temperature group maintained a random distribution (average across all time points: R_n = 0.76 ± 0.02) throughout the time course of the experiment.

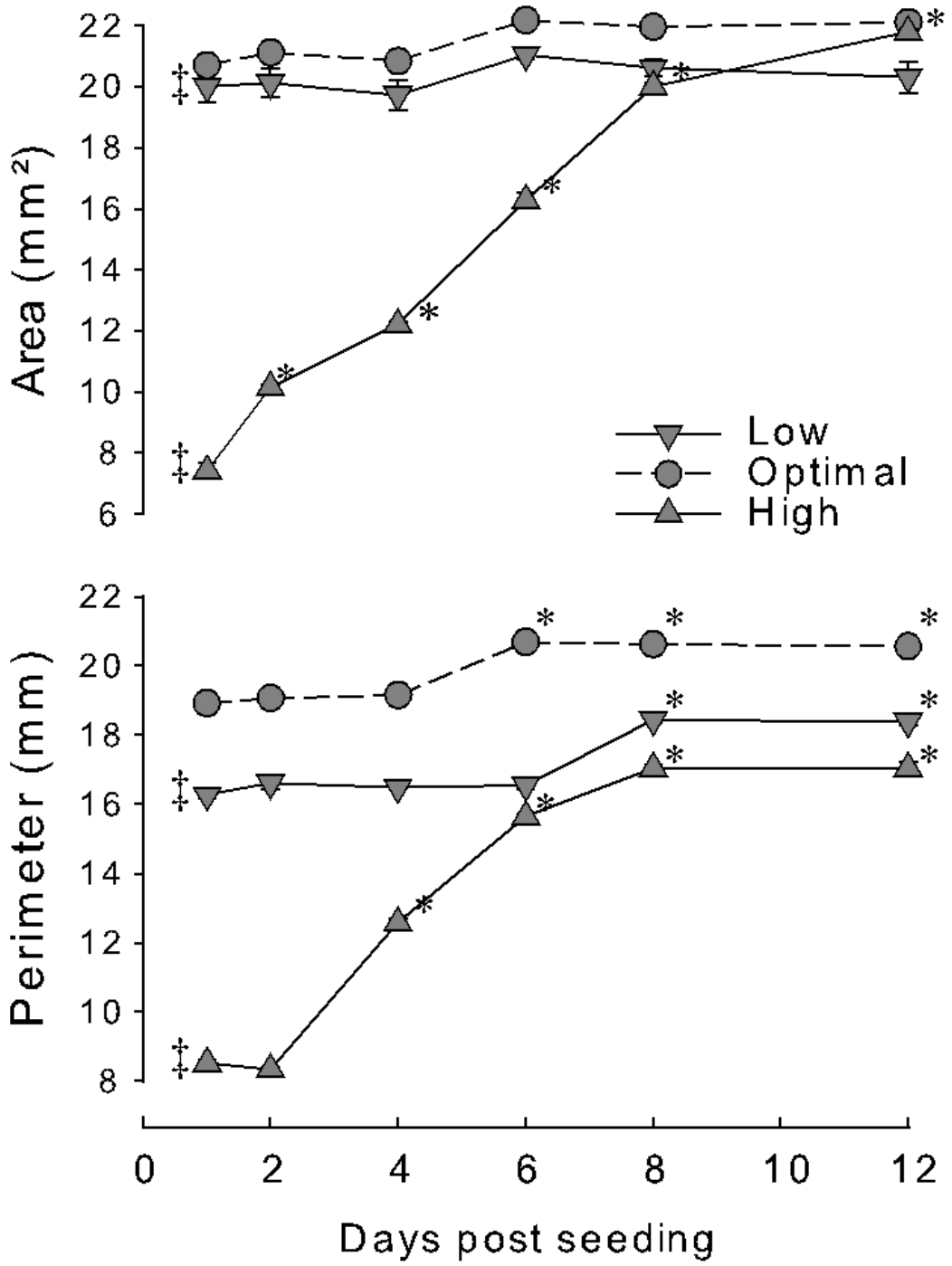

Figure 12: Area (A) and perimeter (B) of human LECs. Cultures grown at the optimal temperature showed the greatest area and perimeter compared to low and high temperatures. When grown at high temperature, the cultures showed a gradual increase in size than those grown at low and optimal temperatures. Double daggers (‡) represent overall differences from those grown at the optimal temperature across the entire time course. Asterisks (*) represent the differences from those grown at 1dps per temperatures.

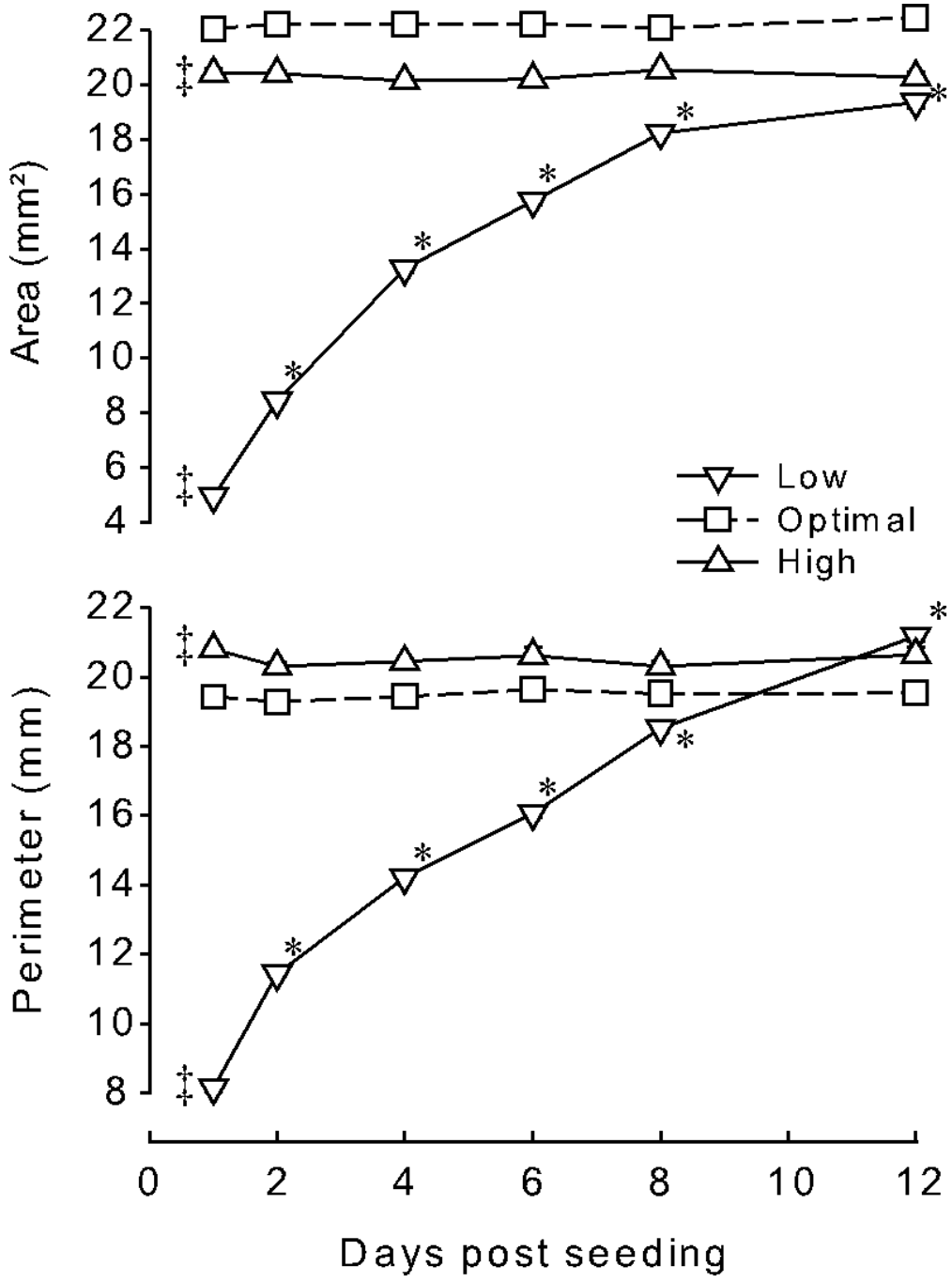

Figure 13: Area (A) and perimeter (B) of fish LECs. Cultures grown at optimal temperatures had significantly greater area compared to non-optimal temperature groups. The perimeter of the cells grown at optimal temperature was significantly less than higher temperature but greater than lowest temperature. A gradual increase in area and perimeter can be seen in cells grown at higher temperature across all experimental days. Double daggers (‡) represent overall differences from those grown at the optimal temperature across the entire time course. Asterisks (*) represent the differences from those grown at 1 dps per temperatures.

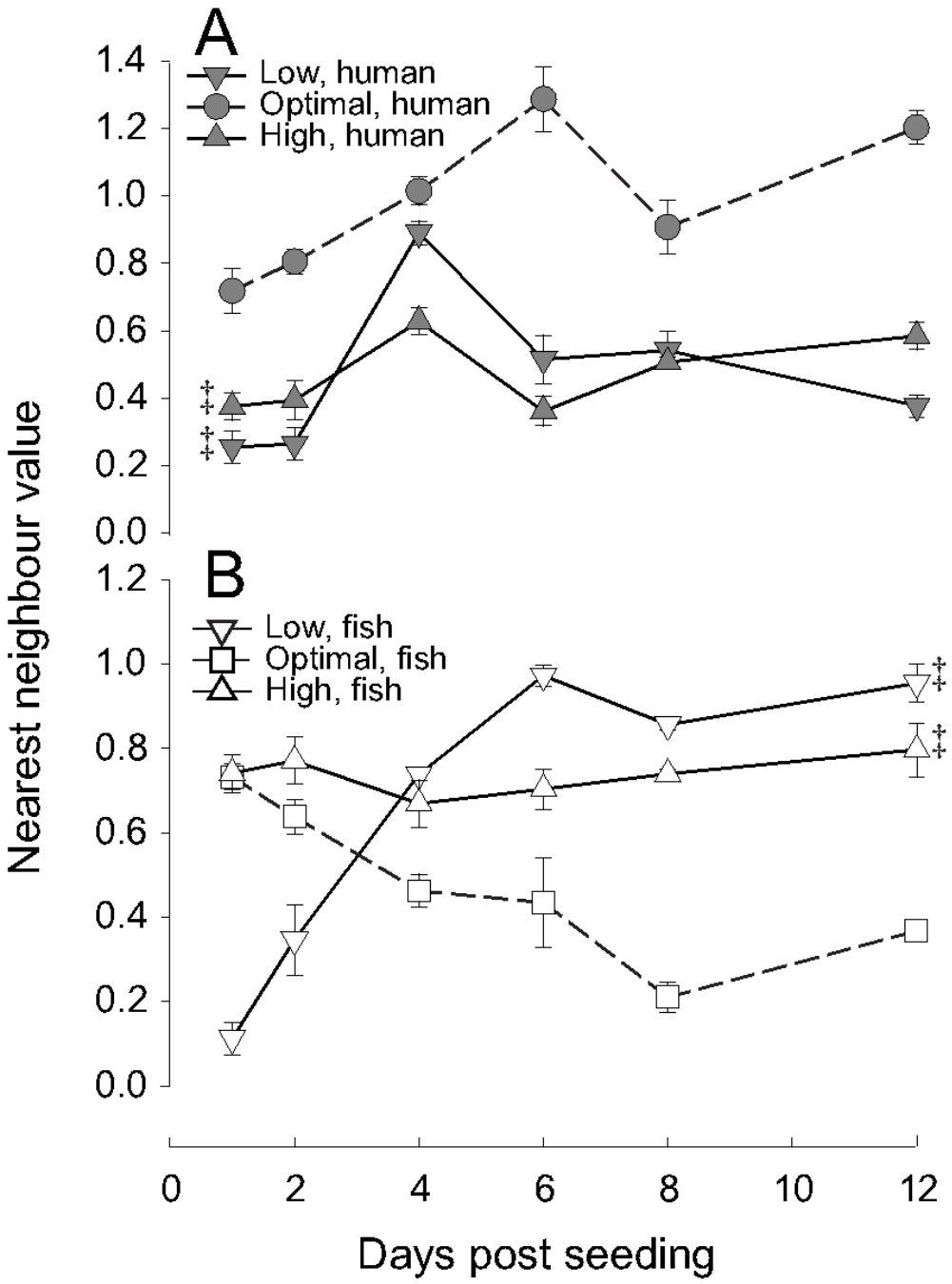

Figure 14: Nearest neighbour value for human (A) and fish (B) LECs. Human LECs grown at non-optimal temperatures were more clumped than optimal temperatures. Fish LECs grown at optimal temperatures initiated as scattered and became more clumped; lowest temperature had the opposite effect. Highest temperature was stable across the experimental time course with randomly scattered distribution. Double daggers (‡) represent overall differences from those grown at the optimal temperature across the entire time course.

V. DISCUSSION

5.1 KEY FINDINGS

5.1.1 Effect of temperature on growth

It is not surprising to see that human cells grew best at the optimal temperatures (Figure 9) yielded the highest number of cells. Mammalian LECs are known to proliferate and develop most rapidly at 36.8°C (McFall-Ngai & Horwitz, 1990). Theoretically speaking, the human LECs should have been more resistant to the heat because α-crystallins have functions that resemble HSPs (de Jong *et al.*, 1993). However, in this study, the performance of the cells was better with lower than higher temperatures (Figure 9), with the cultures grown at the highest temperature faring the worst. In these cultures, prolonged exposure to mild thermal stress could have resulted in changes to the crystallins in the cells. Significant changes occur with α-crystallins; they abandon their activity as chaperones and accumulate around the nucleus as a protective layer (Zhang *et al.*, 2016). However, as the cells eventually adapted to the higher temperature, replication began and the total number and number of mitotic cells started to increase (Figure 9).

Moreover, changes in the growth indices of cells might be affected by other factors. As the experimental days increased, there was a gradual decrease in the total number and number of mitotic of cells stained for cultures at 37°C and 32°C. Given that the cells at the optimal temperature also showed this behaviour, the decrease in mitotic cells may be due to insufficient nutrition or overcrowding.

Rainbow trout are native to the cold waters of the Pacific Ocean and North

America. Rainbow trout can tolerate relatively narrow ranges of temperatures, between 15 to 20°C. Although they do swim up to warmer areas, they use cold refuges (areas with shade) to balance their temperatures. Rainbow trout are affected by warmer temperatures; when directly exposed to temperatures higher than 23°C, they stop growing, and as the temperature rises, oxygen is decreased, which created more stress on the cells (Hartman & Porto, 2014). The proliferation index was the highest for fish LECs that were incubated at optimal temperature, followed by 10°C, then 25°C. As acclimation took effect on the cells at 10°C, the number of mitotic cells increased and proliferation increased. However, due to the low concentration of α-crystallins, the cells did not tolerate heat compared to the cold, resulting in 0% proliferation.

In the beginning, the total number of fish LECs accounted between 18 and 10°C were not significant different from each other. This could be because of the γ-crystallins domination in the fish lens, implying that they are less sensitive of the cold (Posner *et al.*, 2008). However, the number of replicating cells were significantly decreased when grown at 10°C until 6 dps, when the proliferation started to increase (Figure 11). The cells may require time to adapt to the new environment and therefore have no expendable energy to replicate (Brooks *et al*., 2011).

When the cells were incubated at 25°C, there was a high number of DAPI-stained cells across all experimental days; however, there were no mitotic cells (Figure 11). As stated by Chen *et al. (2015)* the critical thermal maximum for rainbow trout is approximately 29°C (depending on their niche). The fishes are able to acclimate to a small range of temperatures, but starting at 25°C is where their aerobic scope (heart rate) decreases to 60% of their optimal (Chen *et al.*, 2015). There may be survival instincts

prior to replication; therefore, the cells maintained their numbers, but did not undergo mitosis.

5.1.2 Effect of temperature on cell morphology and distribution

There may have been a tight junctional change due to the increase in temperature for human LECs. A physiological increase in temperature will cause increase TJ permeability, therefore causing dislocation of many interstitial proteins (Dokladny *et al.*, 2006). This may be the cause of why cells were seen to be smaller than usual and due temperature adaptation, TJ permeability decreased, causing the eventual growth of cells. Tight junctions (TJs) are links between bordering cells that act as barriers, ensuring cell polarity and the regulation of permeability. TJs ultimately seal the interface between cells to prevent leaking (Gumbiner, 1987). These proteins can combine with neighbouring membrane proteins or anchor onto the cytoskeleton.

Fish LECs grew at the optimal temperature, clumping together (Figure 10). Images of the fish LECs also indicated that the amount of cytoplasm was much lower than the humam LECs (compare Figure 7 to Figure 8) , and, unlike the human LECs, which showed typical epithelial cell characteristics, ZO-1 staining was incomplete around the fish LECs (data not shown). Because of their fibroblastic or mesenchymal shape, the area and perimeter of the cells were more difficult to trace, and therefore these values are prone to error.

TJs are very important due to their role in epithelial cells as barriers to prevent the leakage of unwanted proteins. Due to their specific structural integrity, any changes in its conformational arrangement will cause an increase in TJ permeability (Dokladny *et al.*,

2006). There have been studies that show that mesenchymal cells (or mesenchymal-like cells) do not stain well for TJ markers. In mammary gland cells that were either treated with TGF-β1, which induces the transformation of epithelial cells to mesenchymal cells, several epithelial cell markers like E-cadherin, zonula occludins-1 (ZO-1), paxillin, and F-actin were utilized to prove that cell to cell junctions were compromised (Maeda, 2005). The expression of these epithelial cell markers decreased and start to become jagged and harder to recognize (Maeda, 2005).

However, while the ZO-1 markers observed in fish LECs grown at optimal temperatures were jagged and not ideal (data not shown), when fish LECs were grown in 10 and 25°C, the area and perimeter were marked. The cells grown at 10°C started smaller than usual and began to increase in area beginning at 6 dps (Figure 13). At 25°C, on the other hand, cells showed stable area and perimeter measurements across all experimental days (Figure 13).

It should be noted that the size of the fish LECs grown at optimal temperature did not greatly change. The area and perimeter were relatively stable across the time period of the experiment, suggesting that the size of the cells also stayed constant, since the ratio of the area:perimeter, which increases as the radius of the circle increases, did not change greatly (data not shown). Despite the relative stability in size, the cells became more clumped, suggesting a migration of the cells. It is unclear whether a change in shape, such as a rounding up of the cell, could affect the ratio, since rounding up would involve both a decrease in area and perimeter. A true measure would include volumes calculations.

In contrast, the ratio of area:perimeter for LECs at the lowest temperature increased by about 1.5x between 1 dps and 12 dps. In addition, they moved towards a more random distribution. The movement towards a random distribution is the opposite to the LECs grown at optimal temperatures, which tended to clump, and could indicate the beginnings of a mesenchymal to epithelial cell transition (MET). As mentioned above, the TJ staining improved at the later time points, which also points to a MET change, and an increase in cell size associated with cells monolayer is possible but unconfirmed.

Furthermore, if the temperature is above optimal, the metabolism and energy demand for maintenance increases along with higher oxidative pressure. There will be much greater focus on alterations in the antioxidant defence system than on replication. Because of the inability of protein turnover in lens fibres, a lens has a higher vulnerability to reactive oxygen species (ROS) production. Increases in ROS result in oxidative damage and modifications of structural proteins (Remø *et al.*, 2017). This also could have caused the change in cell structure in the fish LECs. Increased oxidative pressure due to changes in nutrient or environment can cause fluctuations in metabolism and growth rates (Remø *et al.*, 2017). It is possible that the stagnant size of the cell, lack of proliferation and lack of movement in the fish LECs grown at the highest temperature reflect the cell's dedication to repair, rather than to migration or replication. However, this concept does not explain the response of the human LECs to higher temperatures. However, it should be noted that human LECs were, at least over the time period assessed, also still capable of replication although at much lower levels.

Given that the patterns for area and perimeter were similar for the human LECs at each temperature, as might be expected, the area:perimeter ratios were not greatly different between the temperatures (average across all time points for lowest, optimal and highest temperatures: 1.189 ± 0.015, 1.084 ± 0.005 and 1.092 ± 0.031, respectively; data not shown), indicating that the sizes of the cells stayed relatively stable.

5.2 CONCLUSION

At optimal temperatures, both fish and human LECs grew optimally. Higher temperatures were more deleterious to the proliferation index than lower temperatures for both human and fish LECs. Mitotic cells were non-existent in fish LECs grown at high temperatures. The sizes of the cells did not greatly change with temperature with either species, but human cells at non-optimal temperature tended to clump over time. Human LECs at the optimal temperature maintained their random distribution. Fish LECs at optimal temperatures moved from a random distribution to a clumped distribution, but lower temperatures had the opposite effect; LECs moved from a clumped to a random distibution. Only the high temperature group of fish LECs maintain their random organisation.

This study could be important for understanding how secondary cataracts develop. It is known that cataracts is the leading cause of blindness in 2018 and posterior capsular opacification (PCO), or secondary cataracts, is the most common reason for reduced vision after cataract surgery (Iliescu *et al.*, 2017). PCO is caused by proliferation by residual lens epithelial cells that were left over from the surgery that causes a secondary opacification (Apple *et al.*, 1992). The rates of observing PCO in children is much

higher than in adults due to the high proliferation rates of lens epithelial cells.

A solution to PCO may be possible if lens epithelial cell growth and control of the behavior of the epithelial cells is understood. If it were possible to decrease the index of proliferation either during or after surgery, it would reduce the chances of patients getting PCO or other complications due to residual LECs. In this research, it is discovered that any change in temperature will cause a decrease in the index of proliferation. In addition, changes to the clumping and possibly the morphology were also observed. Therefore, if the conditions of the surgery were altered so that it reduces the chance of LECs proliferating and migrating, it would decrease the number of patients that has to deal with this complication.

The present study only discussed and analyzed a few of the many uncertainties regarding the LECs of various species. Questions regarding crystallins still remain. Further investigations should seek to determine the distribution of crystallins in various species that are able to live in different environments and to compare the major mechanical or genotypic differences to generate the best solution for humans.

VI. Letters of copyright permissions

FIGURE 1

ELSEVIER

Thank you for your order!

Dear Ms. Ziqing Li,

Thank you for placing your order through Copyright Clearance Center's RightsLink® service.

Order Summary

Licensee:	University of Waterloo
Order Date:	May 9, 2019
Order Number:	4584890547545
Publication:	Elsevier Books
Title:	Clinical Anatomy and Physiology of the Visual System
Type of Use:	reuse in a thesis/dissertation
Order Total:	0.00 CAD

View or print complete details of your order and the publisher's terms and conditions.

Sincerely,

Copyright Clearance Center

Tel: +1-855-239-3415 / +1-978-646-2777
customercare@copyright.com
https://myaccount.copyright.com

Copyright Clearance Center RightsLink®

FIGURE 4

Thank you for your order!

Dear Ms. Ziqing Li,

Thank you for placing your order through Copyright Clearance Center's RightsLink® service.

Order Summary

Licensee:	University of Waterloo
Order Date:	Aug 8, 2019
Order Number:	4644500699674
Publication:	The International Journal of Biochemistry & Cell Biology
Title:	The lens epithelium: Focus on the expression and function of the α-crystallin chaperones
Type of Use:	reuse in a thesis/dissertation
Order Total:	0.00 USD

View or print complete details of your order and the publisher's terms and conditions.

Sincerely,

Copyright Clearance Center

Tel: +1-855-239-3415 / +1-978-646-2777
customercare@copyright.com
https://myaccount.copyright.com

Copyright Clearance Center RightsLink®

VII. References

Abcam. (2015). Counting cells using a hemocytometer. *Protocols*. https://doi.org/10.1038/sj.ejhg.5200954

Adler, R., & Canto-Soler, M. V. (2007). Molecular mechanisms of optic vesicle development: complexities, ambiguities and controversies. *Dev Biol*, *305*(1), 1–13. https://doi.org/10.1016/j.ydbio.2007.01.045

Agarwal, M. L., Agarwal, A., Taylor, W. R., & Stark, G. R. %J P. of the N. A. of S. (1995). *p53 controls both the G2/M and the G1 cell cycle checkpoints and mediates reversible growth arrest in human fibroblasts*. *92*(18), 8493–8497.

Ahrend, M. H. J., Boursa, J., & Födisch, H. J. (1987). Water-soluble and insoluble crystallins of the developing human fetal lens, analyzed by agarose/polyacrylamide thin-layer isoelectric focusing. *Ophthalmic Research*. https://doi.org/10.1159/000265487

Al-Ghadyan, A. A., & Cotlier, E. (1986). Rise in lens temperature on exposure to sunlight or high ambient temperature. *Br J Ophthalmol*, *70*(6), 421–426. Retrieved from https://www.ncbi.nlm.nih.gov/pubmed/3718905

Andley, U. P. (2007). Crystallins in the eye: Function and pathology. *Prog Retin Eye Res*, *26*(1), 78–98. https://doi.org/10.1016/j.preteyeres.2006.10.003

Andley, U. P. (2008). The lens epithelium: focus on the expression and function of the alpha-crystallin chaperones. *Int J Biochem Cell Biol*, *40*(3), 317–323. https://doi.org/10.1016/j.biocel.2007.10.034

Apple, D. J., Solomon, K. D., Tetz, M. R., Assia, E. I., Holland, E. Y., Legler, U. F., … Kostick, A. M. (1992). Posterior capsule opacification. *Surv Ophthalmol*, *37*(2), 73–116. Retrieved from https://www.ncbi.nlm.nih.gov/pubmed/1455302

Augusteyn, R. C. (2004). alpha-crystallin: a review of its structure and function. *Clin Exp Optom*, *87*(6), 356–366. Retrieved from https://www.ncbi.nlm.nih.gov/pubmed/15575808

Augusteyn, R. C. (2010). On the growth and internal structure of the human lens. *Exp Eye Res*, *90*(6), 643–654. https://doi.org/10.1016/j.exer.2010.01.013

Barrio-Asensio, C., Peña-Melián, A., Puerta-Fonollá, J., Vázquez-Osorio, T., & Murillo-González, J. %J V. research. (2002). *Ciliary muscle in avian is derived from mesenchymal and epithelial cells*. *42*(14), 1695–1699.

Bermudez, M. A., Vicente, A. F., Romero, M. C., Arcos, M. D., Abalo, J. M., & Gonzalez, F. (2011). Time course of cold cataract development in anesthetized mice. *Current Eye Research*. https://doi.org/10.3109/02713683.2010.542868

Betz, M. J., & Enerback, S. (2015). Human Brown Adipose Tissue: What We Have Learned So Far. *Diabetes*, *64*(7), 2352–2360. https://doi.org/10.2337/db15-0146

Block, W. (1982). Cold Hardiness in Invertebrate Poikilotherms. *Comparative Biochemistry and Physiology A-Physiology*, *73*(4), 581–593.

Brooks, A. N., Turkarslan, S., Beer, K. D., Yin Lo, F., & Baliga, N. S. (2011). Adaptation of cells to new environments. *Wiley Interdisciplinary Reviews: Systems Biology and Medicine*. https://doi.org/10.1002/wsbm.136

Brown, N. A. P., Vrensen, G., Shun-Shin, G. A., & Willekens, B. (1989). Lamellar separation in the human lens: The case for fibre folds. A combined in vivo and electron microscopy study. *Eye (Basingstoke)*. https://doi.org/10.1038/eye.1989.93

Chen, J., Li, Z., Zhang, L., Ou, S., Wang, Y., He, X., … Yang, S. (2017). Descemet's Membrane Supports Corneal Endothelial Cell Regeneration in Rabbits. *Scientific Reports*, *7*(1), 6983.

Chen, Z., Snow, M., Lawrence, C. S., Church, A. R., Narum, S. R., Devlin, R. H., & Farrell, A. P. (2015). Selection for upper thermal tolerance in rainbow trout (Oncorhynchus mykiss Walbaum). *Journal of Experimental Biology*. https://doi.org/10.1242/jeb.113993

Cooper, G. M. %J T. cell: a molecular approach. (2000). *The eukaryotic cell cycle*.

Cvekl, A., & Tamm, E. R. (2004). Anterior eye development and ocular mesenchyme: New insights from mouse models and human diseases. *BioEssays*. https://doi.org/10.1002/bies.20009

Davis-Silberman, N., & Ashery-Padan, R. (2008). Iris development in vertebrates; genetic and molecular considerations. *Brain Res*, *1192*, 17–28. https://doi.org/10.1016/j.brainres.2007.03.043

de Jong, W. W., Leunissen, J. A., & Voorter, C. E. (1993). Evolution of the alpha-crystallin/small heat-shock protein family. *Mol Biol Evol*, *10*(1), 103–126. https://doi.org/10.1093/oxfordjournals.molbev.a039992

DelMonte, D. W., & Kim, T. (2011). Anatomy and physiology of the cornea. *J*

Cataract Refract Surg, *37*(3), 588–598. https://doi.org/10.1016/j.jcrs.2010.12.037

Dokladny, K., Moseley, P. L., & Ma, T. Y. (2006). Physiologically relevant increase in temperature causes an increase in intestinal epithelial tight junction permeability. *Am J Physiol Gastrointest Liver Physiol*, *290*(2), G204-12. https://doi.org/10.1152/ajpgi.00401.2005

Dolin, P. J. (1994). Ultraviolet radiation and cataract: A review of the epidemiological evidence. *British Journal of Ophthalmology*. https://doi.org/10.1136/bjo.78.6.478

Ellis, R. J., & Hemmingsen, S. M. (1989). Molecular Chaperones - Proteins Essential for the Biogenesis of Some Macromolecular Structures. *Trends in Biochemical Sciences*, *14*(8), 339–342.

Francois, J. (1982). Genetics of cataract. *Ophthalmologica*. https://doi.org/10.1159/000309186

Freeman, R. S., & Donoghue, D. J. (1991). Protein-Kinases and Protooncogenes - Biochemical Regulators of the Eukaryotic Cell-Cycle. *Biochemistry*, *30*(9), 2293–2302. https://doi.org/DOI 10.1021/bi00223a001

Geeraets, W. J. (1972). Observations of Lens Epithelium in Cell-Cultures. *Medical College of Virginia Quarterly*, *8*(4), 264–273.

Griep, A. E. (2006). Cell cycle regulation in the developing lens. *Seminars in Cell and Developmental Biology*. https://doi.org/10.1016/j.semcdb.2006.10.004

Gumbiner, B. (1987). Structure, biochemistry, and assembly of epithelial tight junctions. *Am J Physiol*, *253*(6 Pt 1), C749-58.

https://doi.org/10.1152/ajpcell.1987.253.6.C749

Hamilton, M. E., Bols, N. C., & Duncker, B. P. %J C. (2018). *The characterization of γH2AX and p53 as biomarkers of genotoxic stress in a rainbow trout (Oncorhynchus mykiss) brain cell line*. *201*, 850–858.

Hartman, K. J., & Porto, M. A. (2014). Thermal Performance of Three Rainbow Trout Strains at Above-Optimal Temperatures. *Transactions of the American Fisheries Society*. https://doi.org/10.1080/00028487.2014.945662

Hikida, M., & Iwata, S. (1985). Studies on the eye lens in poikilothermal animals. II. Stimulation of anaerobic glycolysis in rainbow trout lenses incubated with Ca2+-free medium. *Exp Eye Res*, *41*(2), 179–182. Retrieved from https://www.ncbi.nlm.nih.gov/pubmed/2998851

Horwitz, J. (1992). Alpha-crystallin can function as a molecular chaperone. *Proceedings of the National Academy of Sciences*, *89*(21), 10449–10453.

Horwitz, J., Kabasawa, I., & Kinoshita, J. H. (1977). Conformation of gamma-crystallins of the calf lens: effects of temperature and denaturing agents. *Exp Eye Res*, *25*(2), 199–208. Retrieved from https://www.ncbi.nlm.nih.gov/pubmed/913511

Iliescu, I. M., Constantin, M. A., Cozma, C., Moraru, O. M., & Moraru, C. M. (2017). Posterior Capsule Opacification and Nd-YAG rates evaluation in a large series of pseudophakic cases. *Rom J Ophthalmol*, *61*(4), 267–274. Retrieved from https://www.ncbi.nlm.nih.gov/pubmed/29516046

Iwata, S. (1985). Effect of temperature on the rainbow trout lens. *Curr Eye Res*, *4*(4),

441–446. Retrieved from https://www.ncbi.nlm.nih.gov/pubmed/2990820

Jagger, W. S. (1992). The optics of the spherical fish lens. *Vision Res*, *32*(7), 1271–1284. Retrieved from https://www.ncbi.nlm.nih.gov/pubmed/1455702

Johnson, D. G., & Walker, C. L. (1999). Cyclins and cell cycle checkpoints. *Annual Review of Pharmacology and Toxicology*, *39*, 295–312. https://doi.org/DOI 10.1146/annurev.pharmtox.39.1.295

Joukal, M. (2017). Anatomy of the human visual pathway. In *Homonymous Visual Field Defects* (pp. 1–16). Springer.

Joyce, C., & Peterson, D. C. (2019). Neuroanatomy, Cranial Nerve 3 (Oculomotor). In *StatPearls*. Retrieved from https://www.ncbi.nlm.nih.gov/pubmed/30725811

Koning, A. J., Lum, P. Y., Williams, J. M., & Wright, R. (1993). DiOC6 staining reveals organelle structure and dynamics in living yeast cells. *Cell Motility and the Cytoskeleton*. https://doi.org/10.1002/cm.970250202

Kuszak, J., Bertram, B. A., Macsai, M. S., & Rae, J. L. (1984). Sutures of the crystalline lens: a review. *Scan Electron Microsc*, (Pt 3), 1369–1378. Retrieved from https://www.ncbi.nlm.nih.gov/pubmed/6390664

Kuszak, J., Zoltoski, R. K., & Tiedemann, C. E. %J I. J. of D. B. (2004). *Development of lens sutures*. *48*(8–9), 889–902.

Land, M. F. (2005). The optical structures of animal eyes. *Curr Biol*, *15*(9), R319-23. https://doi.org/10.1016/j.cub.2005.04.041

Land, M. F., & Fernald, R. D. (1992). The evolution of eyes. *Annu Rev Neurosci*, *15*,

1–29. https://doi.org/10.1146/annurev.ne.15.030192.000245

Lengsfeld, A. M., Löw, I., Wieland, T., Dancker, P., & Hasselbach, W. (1974). Interaction of phalloidin with actin. *Proceedings of the National Academy of Sciences of the United States of America*. https://doi.org/10.1073/pnas.71.7.2803

Lepcha, N. T., Sharma, I. P., Sapkota, Y. D., Das, T., Phuntsho, T., Tenzin, N., … Peldon, S. (2019). Changing trends of blindness, visual impairment and cataract surgery in Bhutan: 2009-2018. *PLoS One*, *14*(5), e0216398. https://doi.org/10.1371/journal.pone.0216398

Lerman, S., Zigman, S., & Forbes, W. F. (1966). Properties of a cryoprotein in the ocular lens. *Biochem Biophys Res Commun*, *22*(1), 57–61. https://doi.org/10.1016/0006-291x(66)90602-4

Levesque, D. L., & Lovegrove, B. G. (2014). Increased homeothermy during reproduction in a basal placental mammal. *J Exp Biol*, *217*(Pt 9), 1535–1542. https://doi.org/10.1242/jeb.098848

Li, Y., & Ding, Y. (2017). Embryonic Development of the Human Lens. In *Pediatric Lens Diseases* (pp. 1–9). Springer.

Lim, S. H., & Kaldis, P. (2013). Cdks, cyclins and CKIs: roles beyond cell cycle regulation. *Development*, *140*(15), 3079–3093. https://doi.org/10.1242/dev.091744

Liu, W. Y., Wang, Z. B., Zhang, L. C., Wei, X., & Li, L. (2012). Tight junction in blood-brain barrier: an overview of structure, regulation, and regulator substances. *CNS Neurosci Ther*, *18*(8), 609–615. https://doi.org/10.1111/j.1755-

5949.2012.00340.x

Lydahl, E., & Philipson, B. (1984). INFRARED RADIATION AND CATARACT I EPIDEMIOLOGIC INVESTIGATION OF IRON- AND STEEL-WORKERS. *Acta Ophthalmologica*. https://doi.org/10.1111/j.1755-3768.1984.tb06162.x

Maeda, M. (2005). Cadherin switching: essential for behavioral but not morphological changes during an epithelium-to-mesenchyme transition. *Journal of Cell Science*. https://doi.org/10.1242/jcs.01634

Mahler, B., Chen, Y., Ford, J., Thiel, C., Wistow, G., & Wu, Z. (2013). Structure and dynamics of the fish eye lens protein, gammaM7-crystallin. *Biochemistry*, *52*(20), 3579–3587. https://doi.org/10.1021/bi400151c

Mann, I. C. (1928). *The development of the human eye. With a foreword by Sir John Herbert Parsons*. Cambridge: University Press.

Mathis, U., Schaeffel, F., & Howland, H. C. (1988). Visual optics in toads (Bufo americanus). *J Comp Physiol A*, *163*(2), 201–213. Retrieved from https://www.ncbi.nlm.nih.gov/pubmed/3404484

Maurice, D. M. (1957). The structure and transparency of the cornea. *J Physiol*, *136*(2), 263–286. Retrieved from https://www.ncbi.nlm.nih.gov/pubmed/13429485

McAvoy, J. W., Chamberlain, C. G., de Iongh, R. U., Hales, A. M., & Lovicu, F. J. (1999). Lens development. *Eye (Lond)*, *13 (Pt 3b*, 425–437. https://doi.org/10.1038/eye.1999.117

McCaa, C. S. (1982). The eye and visual nervous system: anatomy, physiology and

toxicology. *Environ Health Perspect*, *44*, 1–8. https://doi.org/10.1289/ehp.82441

McFall-Ngai, M. J., & Horwitz, J. (1990). A comparative study of the thermal stability of the vertebrate eye lens: Antarctic ice fish to the desert iguana. *Exp Eye Res*, *50*(6), 703–709. Retrieved from https://www.ncbi.nlm.nih.gov/pubmed/2373164

Meyer-Rochow, V. B., & Pyle, C. A. (1980). Fatty acid analysis of lens and retina of two antarctic fish and of the head and body of the antarctic amphipod Orchomene plebs. *Comparative Biochemistry and Physiology Part B: Comparative Biochemistry*, *65*(2), 395–398.

Michael, R., & Brismar, H. (2001). Lens growth and protein density in the rat lens after in vivo exposure to ultraviolet radiation. *Investigative Ophthalmology and Visual Science*.

Mitchison, J. M., & Carter, B. L. A. %J M. C. B. (1975). *Cell cycle analysis*. *11*, 201–219.

Morgan, D. O. (2007). The cell cycle : principles of control. In *Primers in biology*. LondonSunderland, MA: Published by New Science Press in association with Oxford University Press ;Distributed inside North America by Sinauer Associates, Publishers.

Mutti, D. O., Zadnik, K., & Adams, A. J. (1995). The equivalent refractive index of the crystalline lens in childhood. *Vision Research*. https://doi.org/10.1016/0042-6989(94)00262-K

Neutelings, T., Lambert, C. A., Nusgens, B. V, & Colige, A. C. (2013). Effects of

Mild Cold Shock (25 degrees C) Followed by Warming Up at 37 degrees C on the Cellular Stress Response. *PLoS One*, *8*(7). https://doi.org/UNSP e6968710.1371/journal.pone.0069687

Nickla, D. L., & Wallman, J. (2010). The multifunctional choroid. *Prog Retin Eye Res*, *29*(2), 144–168. https://doi.org/10.1016/j.preteyeres.2009.12.002

Noga, E. J., Wolf, E. D., & Cardeilhac, P. T. %J J. of the A. V. M. A. (1981). *Cataracts in cichlid fish*. *179*(11), 1181–1182.

Nolte, J. (2016). Human Brain: An Introduction to Its Functional Anatomy. In *Elsevier, Inc.*

Oriowo, O. M., Chou, B. R., Cullen, A. P., & Robinson, B. E. (1997). Occupational exposure to optical radiation and the ocular health status of glassblowers. *Ophthalmic and Physiological Optics*. https://doi.org/10.1111/j.1475-1313.1997.tb00087.x

Oyster, C. W. (1999). *The human eye : structure and function*. Sunderland, Mass.: Sinauer Associates.

Pierscionek, B. K., & Augusteyn, R. C. (1995). The refractive index and protein distribution in the blue eye trevally lens. *Journal of the American Optometric Association*.

Pilar, G., Nunez, R., McLennan, I. S., & Meriney, S. D. (1987). Muscarinic and nicotinic synaptic activation of the developing chicken iris. *J Neurosci*, *7*(12), 3813–3826. Retrieved from https://www.ncbi.nlm.nih.gov/pubmed/2826718

Pokorny, J., Smith, V. C., & Lutze, M. (1987). Aging of the human lens. *Applied Optics*. https://doi.org/10.1364/ao.26.001437

Pollard, J. W. (1990). Basic cell culture. *Methods Mol Biol*, *5*, 1–12. https://doi.org/10.1385/0-89603-150-0:1

Pollreisz, A., & Schmidt-Erfurth, U. (2010). Diabetic Cataract—Pathogenesis, Epidemiology and Treatment. *Journal of Ophthalmology*. https://doi.org/10.1155/2010/608751

Posner, M., Hawke, M., LaCava, C., Prince, C. J., Bellanco, N. R., & Corbin, R. W. (2008). A proteome map of the zebrafish (Danio rerio) lens reveals similarities between zebrafish and mammalian crystallin expression. *Molecular Vision*, *14*, 806.

Prince, J. H. (1956). *Comparative anatomy of the eye*. Springfield, Ill.,: Thomas.

Purves, D *et al.*, A. G. J. (2001). Anatomy of the Eye. In *Neuroscience. 2nd edition.* (MA): Sinauer Associates.

Purves, D., Augustine, G., Fitzpatrick, D., Katz, L., LaMantia, A.-S., McNamara, J., & Williams, M. (2001). Neuroscience. 2nd edition.

Rao, K. P. (1963). Physiology of low temperature acclimation in tropical poikilotherms. *Proceedings of the Indian Academy of Sciences-Section B*, *57*(5), 290–296. Springer.

Rastogi, S. C. (2007). *Essentials of animal physiology*. New Age International.

Remington, L. A. (2005). *Clinical anatomy of the visual system* (2nd ed., pp. xi, 292 p.). 2nd ed., pp. xi, 292 p. Retrieved from http://myaccess.library.utoronto.ca/login?url=http://www.sciencedirect.com/science/

book/9780750674904

Remington, L. A., & Remington, L. A. (2012). *Clinical anatomy and physiology of the visual system* (3rd ed., pp. ix, 292 p.). 3rd ed., pp. ix, 292 p. Retrieved from http://myaccess.library.utoronto.ca/login?url=https://www.sciencedirect.com/science/book/9781437719260

Remø, S. C., Hevrøy, E. M., Breck, O., Olsvik, P. A., & Waagbø, R. (2017). Lens metabolomic profiling as a tool to understand cataractogenesis in Atlantic salmon and rainbow trout reared at optimum and high temperature. *PLoS One*, *12*(4), e0175491.

Roper-Hall, M. J. (1977). Traumatic cataract. *Transactions of the Ophthalmological Societies of the United Kingdom*, *97*(1), 58–59.

Rosenbluth, R. F., & Fatt, I. %J E. E. R. (1977). *Temperature measurements in the eye*. *25*(4), 325–341.

Sharon, N., Bar-Yoseph, P. Z., Bormusov, E., & Dovrat, A. (2008). Simulation of heat exposure and damage to the eye lens in a neighborhood bakery. *Exp Eye Res*, *87*(1), 49–55. https://doi.org/10.1016/j.exer.2008.04.007

Sivak, J. G. (1978). A Survey of Vertebrate Strategies for Vision in Air and Water. In *Sensory Ecology*. https://doi.org/10.1007/978-1-4684-3363-0_19

Sivak, J. G. (1990). Optical variability of the fish lens. In R. H. Douglas (Ed.), *The visual system of fish* (pp. 63–80). https://doi.org/https://doi.org/10.1007/978-94-009-0411-8

Sivak, J. G. (2004). Through the lens clearly: phylogeny and development: the Proctor lecture. *Invest Ophthalmol Vis Sci*, *45*(3), 740–747; 739. Retrieved from https://www.ncbi.nlm.nih.gov/pubmed/14985284

Somiya, H., & Tamura, T. (1973). Studies on the visual accommodation in fishes. *Japanese Journal of Ichthyology*, *20*(4), 193–206.

Speakman, J. R. (2001). Thermoregulation in vertebrates: Acclimation, acclimatization and adaptation. *E LS*.

Srinivasan, B. D., & Harding, C. V. (1965). Cellular Proliferation in the Lens. *Invest Ophthalmol*, *4*, 452–470. Retrieved from https://www.ncbi.nlm.nih.gov/pubmed/14340161

Tan, C. L., & Knight, Z. A. (2018). Regulation of Body Temperature by the Nervous System. *Neuron*, *98*(1), 31–48. https://doi.org/10.1016/j.neuron.2018.02.022

Taylor, V. L., al-Ghoul, K. J., Lane, C. W., Davis, V. A., Kuszak, J. R., & Costello, M. J. (1996). Morphology of the normal human lens. *Invest Ophthalmol Vis Sci*, *37*(7), 1396–1410. Retrieved from https://www.ncbi.nlm.nih.gov/pubmed/8641842

ThermoFisher Scientific Inc. (2010). Gibco Cell Culture Basics Handbook. In *ThermoFisher Scientific Inc.* https://doi.org/10.1093/chemse/bjt099

Van Buskirk, E. M. (1989). The anatomy of the limbus. *Eye (Lond)*, *3 (Pt 2)*, 101–108. https://doi.org/10.1038/eye.1989.16

Vendra, V. P., Khan, I., Chandani, S., Muniyandi, A., & Balasubramanian, D. (2016). Gamma crystallins of the human eye lens. *Biochim Biophys Acta*, *1860*(1 Pt B),

333–343. https://doi.org/10.1016/j.bbagen.2015.06.007

Voaden, M. J. (1971). Effect of temperature on cell division in the cultured rabbit lens. *Exp Eye Res*, *11*(1), 7–14. Retrieved from https://www.ncbi.nlm.nih.gov/pubmed/5130523

Vos, J. J., & van Norren, D. (2004). Thermal cataract, from furnaces to lasers. *Clin Exp Optom*, *87*(6), 372–376. Retrieved from https://www.ncbi.nlm.nih.gov/pubmed/15575810

Walls, G. L. (1942). The vertebrate eye and its adaptive radiation. In *Bulletin / Cranbrook Institute of Science ;* Bloomfield Hills, Mich.: Cranbrook Institute of Science.

Warrant, E. J. (2017). The remarkable visual capacities of nocturnal insects: vision at the limits with small eyes and tiny brains. *Philos Trans R Soc Lond B Biol Sci*, *372*(1717). https://doi.org/10.1098/rstb.2016.0063

West, J. A., Sivak, J. G., & Moccia, R. D. (1994). Embryology of the Teleost (Oncorhynchus-Mykiss) Lens. *Canadian Journal of Zoology-Revue Canadienne De Zoologie*, *72*(4), 689–701. https://doi.org/DOI 10.1139/z94-093

WHO. (2018). Visual impairment and blindness. *World Health Organization*. https://doi.org/10.1007/SpringerReference_61253

Willekens, B., & Vrensen, G. (1982). The three-dimensional organization of lens fibers in the rhesus monkey. *Graefe's Archive for Clinical and Experimental Ophthalmology*. https://doi.org/10.1007/BF02152295

Wilson, S. E., & Hong, J. W. (2000). Bowman's layer structure and function: critical or dispensable to corneal function? A hypothesis. *Cornea*, *19*(4), 417–420. Retrieved from https://www.ncbi.nlm.nih.gov/pubmed/10928749

Wise, C. (2002). Epithelial cell culture protocols. *Methods in Molecular Biology ; 188*, pp. xiv, 405 p. Retrieved from http://myaccess.library.utoronto.ca/login?url=http://ebookcentral.proquest.com/lib/utoronto/detail.action?docID=3036832

Zhang, K., Zhu, X., & Lu, Y. (2016). Effect of Mild Heating on Human Lens Epithelial Cells: A Possible Model of Lens Aging. *Scientific Reports*, *6*, 33917.

Zhao, H., Brown, P. H., Magone, M. T., & Schuck, P. (2011). The molecular refractive function of lens gamma-Crystallins. *J Mol Biol*, *411*(3), 680–699. https://doi.org/10.1016/j.jmb.2011.06.007

VIII. APPENDIX

6.1 TECHNIQUES UTILIZED

6.1.1 Passage

Routine passaging and seeding were performed using 1% TryPLE Express (Fisher Scientific 12604021). The human and fish LECs were then incubated at 37°C and room temperature, respectively, and viewed under a microscope to determine whether they had dissociated from the surface of the culture flask. The cells were rinsed with twice the volume of culture medium as the TryPLE Express before centrifuging at 500 relative centrifugal force (rcf) (or 1667 rotations per min (rpm) for 5 min at room temperature. The supernatant was decanted, and the cell pellet was thoroughly mixed with new media. This mixture was then divided in half, transferred to a flask or plate, and incubated at the specific temperature required. Notably, all solutions were at room temperature before being added to prevent cold shock and damage to the cells.

6.1.2 Cell counting

A haemocytometer was used to count the cells that were isolated from the flasks via centrifugation. A haemocytometer is a piece of glass that has a counting surface with a coverslip over the top that can hold the cells in suspension. Cell pellets were resuspended in 1 ml of culture medium, and 10 μL of this suspension was added to the haemocytometer between the grid and coverslip. The cells were counted by choosing one of the corner squares and taking the cells that were touching the top, bottom, or side rulings into consideration. Once the total number of cells were counted, the following equation was used to calculate the total cell number:

Total cells/ml = total cells counted * (dilution factor/number of squares) * (1×10^4) cells/ml (Abcam, 2015; Pollard, 1990).

6.1.3 Cryopreserving cells

Before freezing the cells, an essential general check under the microscope for bacterial and fungal infections was performed, which ensured that there were approximately $5 \times 10^6 - 2 \times 10^7$ cells/ml. This was crucial because the cells were going to be reused in the future. Furthermore, infections could lead to unexpected morphological or physiological changes as well as cross-contamination of other healthy vials. While the cells were centrifuged at 500 rcf (or 1,667 rpm), freezing medium was created using 10% (v/v) DMSO with 20% FBS in either DMEM/F-12 or L-15 (ATCC, 2018). After centrifugation, the supernatant was discarded, and the freezing medium was added to the pellet, which was then resuspended to ensure that the final volume contained $1 \times 10^6 - 5 \times 10^6$ cells/ml. Aliquots of 1 ml were added to each cryogenic vial. To avoid contamination, each vial was sealed with parafilm on the exterior. The vials were stored in an Mr.frosty^{tm} freezing container (thermoscientific™) at −80°C. Once completely frozen, the vials were transferred to liquid nitrogen for long-term storage.

6.2 PRELIMINARY TRIALS

6.2.1 Optimal incubation time of EdU

The EdU staining proliferation kit (ifluor 488; Abcam, ab219801) provided a protocol instructing incubation of EdU with cells for 2 to 4 h; tests on EdU incubated in lines for 1, 2, 3, 4, and 5 h were conducted. Once the incubation time had been reached, the protocol was followed. Cells were plated at a density of 3×10^5 cells/ml in the center of 35 mm

glass-bottom Petri dishes and settled overnight with 2 ml of growth media. At the time the dishes were used, 1 ml of the growth media was extracted, and 100 μL of 2X EdU solution was added to yield a 1X EdU solution. Furthermore, 1X fixative of 2 ml of solution was added, and then cells were incubated in the dark for 15 min at room temperature. The cells were then washed twice with a wash buffer (3% BSA with PBS), and then 200 μL of 1X permeabilization buffer was added; the cells were incubated at room temperature for 20 min and washed again with 3% BSA solution three times for 5 min. A reaction mixture was created using 1,720 μL of Tris Buffered Saline (TBS), 80μL of $CuSO_4$, 4.8 μL of ifluor 488 azide, and 200 μL of 1X EdU additive solution, by diluting 10X reaction buffer with miliq water at a ratio of 1:10; 2 ml of the reaction mixture was added to the dishes before being incubated in the dark for 30 min at room temperature. Cells were washed once with the wash buffer and once with PBS. Then, 200 μL of 4′,6-diamidino-2-phenylindole (DAPI) (working solution of 1 μg/ml, Abcam, ab104139) was added for 15 min, and the mixture was protected from light by covering the plates in a dark box. DAPI is a fluorescent nuclear counterstain with excitation and emission properties of 350 and 470 nm, respectively. The cells were washed twice with PBS and mounted on a slide using Prolong Gold Antifade (Sigma, P36930) or Fluoroshield Mounting Medium with DAPI and secured using clear nail polish. The slides were then taken into the Cytation 5 (biotek, cell imaging multi-mode reader), and their mean fluorescence intensities were measured (Table 2).

6.2.2 Optimization of EdU proliferation assay volumes

Smaller amounts of each reagent were used to ensure that more tests could be conducted

Table 2: Mean fluorescent intensities for EdU. The suggested time to incubate cells with EdU varies from 1–5 h in the manual. To find the optimal incubation duration and determine whether EdU itself causes an increase in the index of proliferation, the following test was conducted. Note that when the cells were incubated for 3 h, it yielded the highest mean fluorescent intensity measured by counts per second (cps) as well as the optimal appearance.

Time (h) EdU sits with cells	Mean fluorescent intensity (cps)	Description
1	57	Cells were not stained
2	224	Colour of the cells were moderate
3	1340	Cells were bright green with great detail that was able to trace to find the perimeter
4	112	Some of the cells shrunk and started to crack
5	71	Large puncturing holes were found in the cells

with one kit. The procedures were as noted by the manufacturer but volumes used differed. For plating, 35-mm dishes were used with a 14-mm coverslip (MatTek Corp, P35GCOL-1.5-14-C); thus, the amount of each item required was altered to ensure that there was enough for more than 50 tests. The cells were plated with 200 μL of media and incubated until they had reached 80–90% confluence. A volume of 100 μL of the original media was discarded, and the cells were treated with 0.2 μL 2X EdU stock solution. Human and fish cells were then incubated at their respective optimal temperatures (37°C and 18°C) for 3 h. The contents were aspirated, 200 μL of 1X fixative solution was added, and cells were incubated in the dark for 15 min at room temperature. Plates were then washed (3x5 min) with buffer (3% BSA in PBS) and then 200 μL of 1X permeabilization buffer was added for 20 min at room temperature. Cells were then washed (3x5 min) with buffer (3% BSA in PBS), and the supernatants was aspirated and discarded.

The reaction mixture required for the EdU reaction was created using 86 μL of TBS, 4 μL of $CuSO_4$, 0.24 μL of ifluor 488 azide, and 10 μL of 1X EdU additive solution per test, creating a final volume of 100.24 μL per 35-mm glass-bottom Petri dish. This volume was the correct amount to cover the 14-mm-diameter glass coverslip. Kim wipes were soaked in distilled water and placed in the incubator to maintain the moisture necessary to prevent the cells from drying out. Each plate was incubated in a dark box for 30 min. The cells were then washed (3x5 min) with wash buffer (3% BSA in 1% PBS) and once with PBS. Lastly, 100 μL of DAPI was added to the cells, which were then incubated for 15 min at their optimal growth temperatures, protected from light.

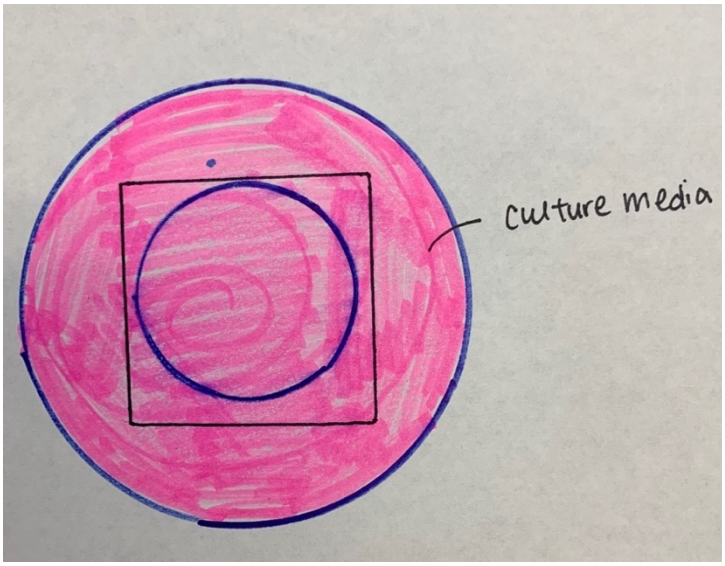

Figure 15: Representation of cell culture prior to optimization. The pink shaded area represents where the original culture medium and cells were seeded. It was unnecessary to use additional medium and cells because we were only going to mount the removeable square slide. Picture was drawn and not to scale.

6.2.3 Cell viability and cytoskeleton test

Various mixtures of dyes were used to determine which was superior for analyzing and

counting the number of cells on the coverslip. 3,3′-dihexyloxacarbocyanine iodide (DIOC(6)) stains the mitochondria to determine which cells are alive (Koning *et al.*, 1993). Phalloidin is a fluorescent dye that stains actin filaments in the cell (Lengsfeld *et al.*, 1974).

The cells were plated onto the 35 mm glass-bottom Petri dishes, settled, and attached overnight. The media were removed, and the cells were fixed by adding 200 μL of 4% paraformaldehyde (PFA) to each for 10 min, followed by incubation. The cells were washed (3x5 min) with PBS, and then permeabilized with 200 μL of 0.1% Triton X-100 for 15 min. Cells were washed again (3x5 min) with PBS, and then 200 μL of DIOC(6) (2 μg/ml working solution) or phalloidin (5 μg/ml working solution) was added for 10 min, incubated at their optimal temperatures, and protected from light. Plates were washed (3x5 min) with PBS, and then 200 μL of DAPI was introduced for 15 min and incubated in a dark place. Finally, these cells were handed with 3x5 min PBS wash, and then mounted on a slide using Prolong Gold Antifade (Sigma, P36930) and secured with clear nail polish.